# Degradation Study of Cu-SSZ-13 Selective Catalytic Reduction Catalysts

---

A

Dissertation

Presented to

the faculty of the School of Engineering and Applied Science
University of Virginia

---

in partial fulfillment

of the requirements for the degree

Doctor of Philosophy

by

Yu-Ren Chen

January 2023

# APPROVAL SHEET

This

Dissertation

is submitted in partial fulfillment of the requirements
for the degree of

Doctor of Philosopy

Author: Yu-Ren Chen

This Dissertation has been read and approved by the examining committee:

Advisor: William Epling

Advisor:

Committee Member: Robert Davis

Committee Member: Christopher Paolucci

Committee Member: Sen Zhang

Committee Member: Giri Gaurav

Committee Member:

Committee Member:

Accepted for the School of Engineering and Applied Science:

Jennifer L. West, School of Engineering and Applied Science

January 2023

**Acknowledgements**

First, I would like to thank my advisor, Prof. William S. Epling. When I failed and was down multiple times in my PhD life, he gave me positive energy and encouraged me to face the challenges. I could not finish my PhD without his encouragement and support. In addition, his fruitful ideas always enlighten me, and his teaching style gives me different angles to see through a problem. He equipped me all the tools to become a better researcher. I am very thankful to become one of his students.

Next, I would like to thank Prof. Robert J. Davis and Prof. Christopher Paolucci. They pointed out problems in my research during group meetings, gave me different opinions when I interpreted my data, and gave me lessons when I was confused in the discussions. These are valuable experiences in my PhD journey.

I would like to thank all my lab members, Dr. Yasser Jangjou, Dr. Yuntao Gu, Dr. Ryan Zelinsky, Silvia Marino, Sugandha Verma, Carlos Weiler, Fatima Mahnaz, Natalia Diaz Montenegro, and Kanika Meena. Thank you for helping me when I faced problems and welcomed me like I was in a big family. I want to give special thanks to Silvia and Sugandha. Thank you for fully supporting and helping me at the end of my PhD journey. I also want to thank all the postdoctoral researchers and visiting scholars, Dr. Marina Cortés-Reyes, Dr. Lai Wei, Dr. Zhuoran Gan, Dr. Poonam Rani, Prof. Izabela Pieta, Sergio Monlina Ramírez, Umberto Iacobone, and Costanza Preziosi. I would like to thank all of you for giving me help and support, especially for Dr. Marina Cortés-Reyes and Dr. Lai Wei, in my PhD journey. Thank you for making my PhD life wonderful. Finally, I want to thank Keka Mandal and Asanka Wijerathne who cooperated with me in the new project. Thank you for helping me and giving me research input. I also want to thank all the students in Prof. Paolucci and Prof. Davis groups, especially for Dr. Lu Yang, Dr. Gordon

Brezicki, Colby Arthur Whitcomb, and Konstantin Mamedov. Thank you for inspiring me and teaching me all the characterization techniques I need.

I want to thank my funding company Cummins Inc. and researchers in the company, Dr. Ashok Kumar, Dr. Di Wang, Dr. Rohil Daya, and Dr. Krishna Kamasamudram. Thank you for funding my PhD project and giving me research guidance. I also want to thank my internship manager, Abraham J Yanez-Mckay, and the SPA team in Cummins. Thank you for the internship opportunity and a chance to work with talented people. I have learned a lot during the internship.

I am extremely lucky to have so many Taiwanese people around when I first came to UVA. I want to give special thanks to Dr. Kevin Chang. He took care of me when I first came to UVA. He also inspired me how to become a better researcher. I am grateful to have him as my senior and as my important friend.

Finally, I want to thank my parents who allowed me to study abroad. I feel very sorry that I could not go back to Taiwan and see my parents in these past three years because of the pandemic. I am grateful that they fully understood this and unconditionally supported me physically and mentally in my PhD life, especially during the pandemic. I can only say thank you from the bottom of my heart.

**Abstract**

$NO_x$ reduction in a diesel engine after-treatment is challenging. Unlike three-way catalysts in a gasoline engine that operate under stoichiometric conditions, where $NO_x$ can react with stoichiometric amounts of CO and hydrocarbons, in diesel exhaust there is an excess of $O_2$ under which conditions three-way catalysts are ineffective at reducing $NO_x$. The current solution for $NO_x$ reduction in diesel engine exhaust is selective catalytic reduction of $NO_x$ by $NH_3$ ($NH_3$-SCR). The current commercialized catalyst for the $NH_3$-SCR reaction is Cu-SSZ-13.

Even though many advantages can be found with Cu-SSZ-13 catalysts compared to others, sulfur poisoning is still a problem. In this work, we first measured SCR and $NH_3$, NO, CO, and $SO_2$ oxidation performance after $SO_2$ or $SO_2$ + $SO_3$ exposure on catalysts that had been exposed to mild hydrothermal aging conditions. We found there is a strong correlation between the extent of sulfur poisoning and the catalyst oxidation ability. The results suggest that with a great extent of $SO_2$ oxidation, or more oxidation of $SO_x$ species on the catalyst surface, more extensive catalyst poisoning occurs.

Next, we studied which Cu species were more strongly affected by sulfur. Calculations performed by Keka Mandal, Asanka Wijerathne and Professor Paolucci suggest that Cu dimers strongly bind sulfur. A CO titration method and diffuse reflectance ultra-violet spectroscopy (DR UV-Vis) were used to evaluate a change in amount of static Cu dimers sites before and after sulfur exposure. We found out that Cu dimers were lost after $SO_2$ or $SO_2$ + $SO_3$ exposure and there appear to be at least two different Cu/sulfur species based on different impacts of regeneration after $SO_2$ or $SO_2$ + $SO_3$ exposure conditions.

Finally, we studied if different exhaust gas components might have different effects on mild hydrothermal aging. We found that mild hydrothermal aging with ethylene can lead to different oxidation conversion and slightly different high-temperature SCR performance compared to mild hydrothermal aging without any in the exhaust mixture. We believe this is due to different Cu site distributions during mild hydrothermal aging with and without ethylene. We further propose that during mild hydrothermal aging with ethylene, Z2Cu can be transformed back to ZCuOH.

**Table of Contents**

**List of Figures**

**List of Tables**

# Chapter 1. Introduction and Background

## 1.1 Diesel engine

Internal combustion engine vehicles are widely used. Fuel is combusted in a chamber and the high temperature and pressure produced during combustion expands the combustion gases, which applies force to a piston and forces the piston to move, and this mechanical energy is used to move the vehicle. The chemical energy stored in the fuel thus converts to mechanical energy, powering the vehicles.

Diesel and gasoline engines are two common types used in internal combustion engine vehicles. The differences between these two engines are different air-to-fuel ratios and how combustion is induced. The diesel engine is a compression-ignition engine. Air is injected to a combustion chamber and compressed to raise temperature. Because the temperature is so high, when injected, the fuel is ignited. High air-to-fuel ratios are used, ranging from near stoichiometric at 14:1 to as high as 25:1 [1]. The gasoline engine is a spark-ignition engine. Air is mixed with fuel and injected into a combustion chamber and the fuel is ignited by a spark. High air-to fuel ratios, those beyond the stoichiometric amount, are not used [1].

## 1.2 Diesel engine emissions and regulations

The diesel engine is more fuel efficient compared to the gasoline engine and therefore it generates less carbon dioxide ($CO_2$) [2]. Due to the inhomogeneous mixing of air and fuel in the combustion chamber, there is incomplete combustion of fuel which leads to soot, some unburned hydrocarbons, and carbon monoxide (CO). In addition, high temperature and pressure inside the combustion chamber provide an environment for nitrogen oxides ($NO_x$) production, which includes nitric oxide (NO) and nitrogen dioxide ($NO_2$). Nitrogen ($N_2$) and oxygen ($O_2$) is usually

inert in air, but they react when the temperature is high enough through the Zeldovich mechanism [3]. Sulfur dioxide ($SO_2$) is another common emission. Sulfur compounds are in the diesel fuel and the lubricant oil. S levels in the fuel are regulated to under 15 ppm [4].

These emissions can lead to environmental and health problems if not properly treated. To evaluate these emissions, a common method used is the federal test procedure (FTP) for heavy-duty vehicles, defined by the Environmental Protection Agency (EPA). The test was developed to take into account the driving patterns of different trucks and buses in different cities. The testing cycles include New York Non-Freeway (NYNF), Los Angeles Non-Freeway (LANF), Los Angeles Freeway (LAFY), and a repetition of the first NYNF. The cycle is described in Fig. 1.1 [5]. In terms of light-duty vehicles, the FTP-75 is commonly used. The testing cycle includes a cold start transient phase, stabilized phase, and a hot start phase. The cycle is described in the Fig. 1.2 [6].

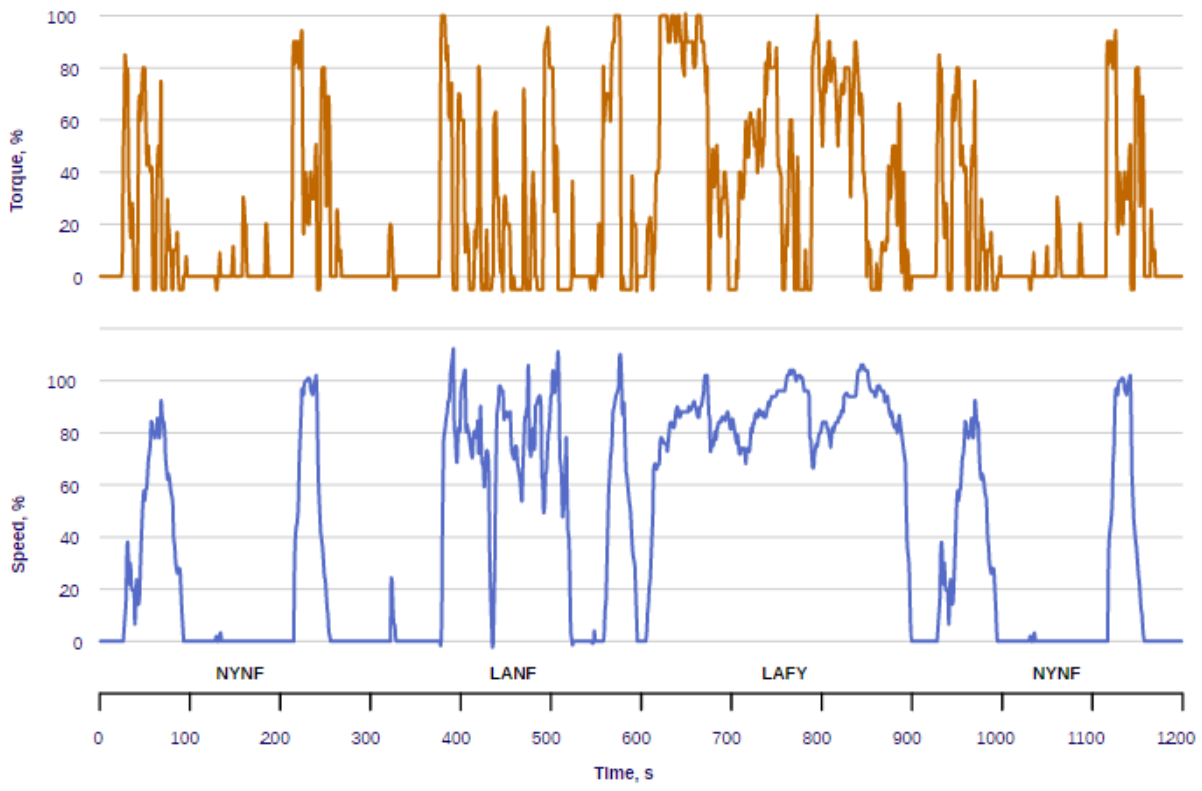


Fig. 1.1. Heavy-duty FTP transient cycle.

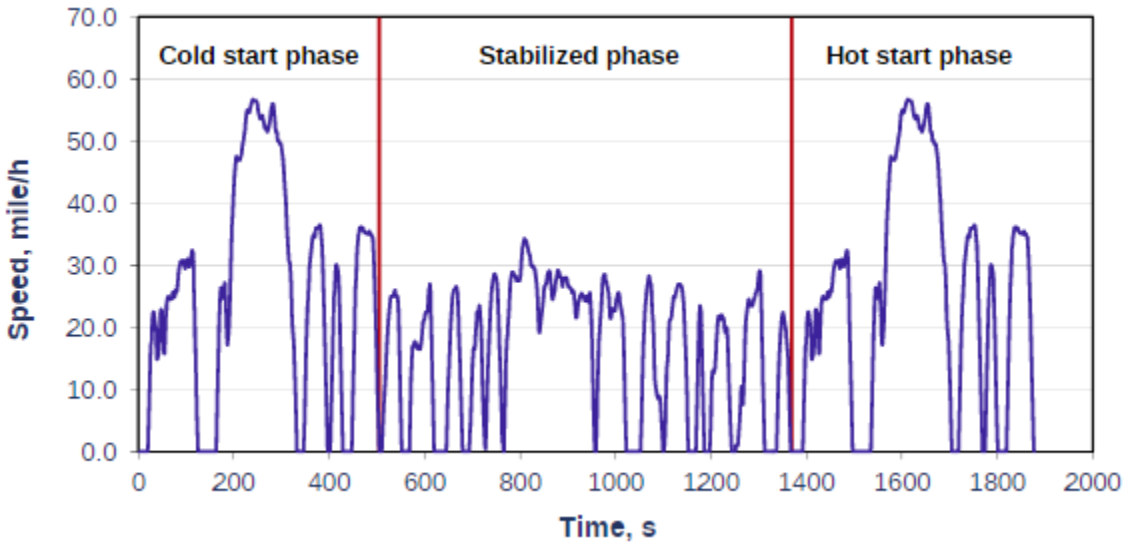


Fig. 1.2. US EPA urban dynamometer driving schedule (FTP-75).

The current regulation for an on-road vehicle is the Tier 3 emission standards. It includes non-methane organic gasses (NMOG), $NO_x$, and particulate matter (PM) standards for light and heavy-duty vehicles, with an end date to meet these of 2025. These standards are meant to reduce volatile organic compounds and $NO_x$ by 80% and PM by 70% compared to 2014 levels, if the vehicle and fuel quality are meeting the standards [7]. The Tier 3 regulations plots of NMOG + $NO_x$ for light-duty and heavy-duty vehicles are shown in 1.3 (a) and (b).

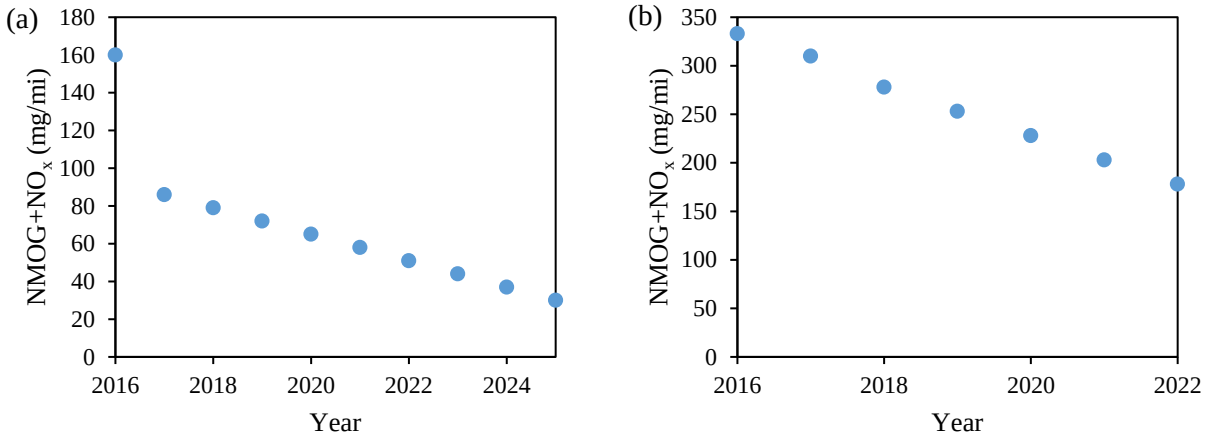


Fig. 1.3. Tier 3 regulations of average federal test procedure (FTP) NMOG + $NO_x$ standards for (a) light-duty vehicles and (b) heavy-duty vehicles [7].

### 1.3 Diesel engine after-treatment

To meet these emission regulations, a catalytic after-treatment system is currently used to reduce emissions from a diesel engine. Although the arrangement and setup might differ, typically it includes a diesel oxidation catalyst (DOC), a diesel particular filter (DPF), a selective catalytic reduction (SCR) catalyst, and an ammonia slip catalyst (ASC). The DOC is mainly used to oxidize unburned hydrocarbons and CO into $CO_2$ and water ($H_2O$). It also oxidizes NO to $NO_2$ and $SO_2$ to sulfur trioxide ($SO_3$). The DPF is used to filter soot. The SCR catalyst is used to reduce $NO_x$ by using ammonia ($NH_3$), which comes from urea decomposition. Lastly, the ASC is used to oxidize

any residual $NH_3$ slipping by the SCR catalyst. Even though the current technologies have improved over the last two decades, and they meet the current regulations, more stringent regulations in future years drive the need for catalyst research and improvement.

### 1.4 $NH_3$-SCR chemistry

$NO_x$ reduction in the diesel engine after-treatment is challenging. The traditional three-way catalyst used in gasoline engine after-treatment is not sufficient to reduce $NO_x$ in diesel engine exhaust because the excess $O_2$ removes reductants that would otherwise be used to reduce $NO_x$. The current solution for $NO_x$ reduction is the selective catalytic reduction of $NO_x$ by $NH_3$ ($NH_3$-SCR). This technique requires $NH_3$ as a reductant, as mentioned above from the decomposition of injected urea into the exhaust upstream of the SCR catalyst. The urea decomposition includes two different steps, thermolysis of urea and hydrolysis of isocyanic acid, shown in the following equations [8,9]:

$$(NH_2)_2CO \rightarrow NH_3 + HNCO \quad (1\text{-}1)$$

$$HNCO + H_2O \rightarrow NH_3 + CO_2 \quad (1\text{-}2)$$

The SCR reactions consist of standard SCR, fast SCR, and $NO_2$ SCR reactions, depending on the $NO_2$ to NO ratio. $NO_2$ is not common in the diesel exhaust, but the DOC can oxidize NO into $NO_2$ and increase the $NO_2$ to NO ratio. If the $NO_2$ to NO ratio in the feed is low, standard SCR is the normal reaction considered [10,11]. The reactions are listed below:

$$4NH_3 + 4NO + O_2 \rightarrow 4N_2 + 6H_2O \text{ (standard SCR)} \quad (1\text{-}3)$$

$$2NH_3 + NO + NO_2 \rightarrow 2N_2 + 3H_2O \text{ (fast SCR)} \quad (1\text{-}4)$$

$$4NH_3 + 2NO_2 + O_2 \rightarrow 3N_2 + 6H_2O \text{ ($NO_2$ SCR)} \quad (1\text{-}5)$$

Other than the main SCR reactions, there are several side reactions that might occur. The most notable side reaction is $NH_3$ oxidation which becomes significant at higher temperatures. In addition, $NH_3$ oxidation can lead to undesired product, NO. Possible $NH_3$ oxidation reactions are shown below [10,12,13]:

$$4NH_3 + 3O_2 \rightarrow 2N_2 + 6H_2O \quad (1\text{-}6)$$

$$4NH_3 + 5O_2 \rightarrow 4NO + 6H_2O \quad (1\text{-}7)$$

Other side reactions, such as NO oxidation and nitrous oxide ($N_2O$) formation can occur. The NO oxidation reaction is shown in (1-8). $N_2O$ is a byproduct of $NH_3$-SCR reactions. In general, $N_2O$ can be formed in two different temperature regions. At lower temperatures (<300 °C), $N_2O$ is generated by ammonium nitrate ($NH_4NO_3$) decomposition [10,14], while at higher temperatures (>300 °C), $N_2O$ is generated from $NH_3$ oxidation. The reactions for these two regions are shown in equations (1-9) to (1-11) [10].

$$2NO + O_2 \rightarrow 2NO_2 \text{ (NO oxidation)} \quad (1\text{-}8)$$

$NH_4NO_3$ generation and decomposition to $N_2O$ at low temperatures [10]:

$$2NH_3 + 2NO_2 \rightarrow NH_4NO_3 + N_2 + H_2O \quad (1\text{-}9)$$

$$NH_4NO_3 \rightarrow N_2O + 2H_2O \quad (1\text{-}10)$$

$NH_3$ oxidation to $N_2O$ at high temperatures [10]:

$$2NH_3 + 2O_2 \rightarrow N_2O + 3H_2O \quad (1\text{-}11)$$

## 1.5 $NH_3$-SCR catalysts

To effectively drive $NH_3$-SCR reactions to reduce $NO_x$, catalysts are important. Early in SCR research, the $V_2O_5$-$WO_3$-$TiO_2$ catalyst was used. The optimum operation temperature of this catalyst is reported to be between 300 to around 400 °C [15]. However, many drawbacks of the catalyst were found, such as low high temperature stability and toxicity of the catalyst. Zeolite-based catalysts were used as alternatives. Among all the zeolite-based catalysts, SSZ-13 and SAPO-34 received most attention because of hydrothermal stability at high temperatures, resistance to hydrocarbon poisoning, and wide working temperature windows compared to other zeolites, such as Zeolite Y, ZSM-5, and beta [16]. In terms of active metal, Fe and Cu are the most common choices [17-34]. Higher SCR conversion at high temperatures is mostly observed on Fe catalysts compared to Cu catalysts. However, lower SCR conversion at low temperatures compared to Cu catalysts is the drawback, see Fig. 1-4 [15]. The common working temperatures for SCR reactions in heavy-duty vehicles are between 200 to 400 °C [5]. For this reason, Cu-based catalysts are more commonly selected for the SCR catalyst.

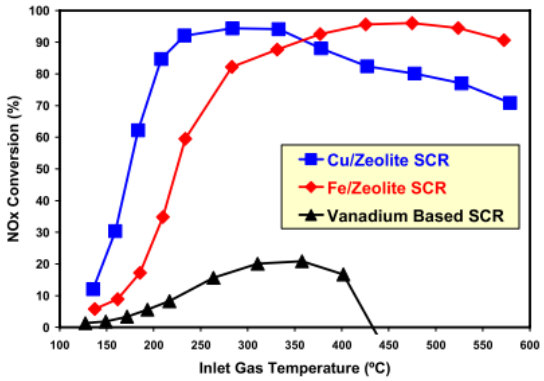


Fig. 1.4. $NO_x$ conversion over Cu, Fe, and vanadium based SCR reaction as a function of temperature [15].

Cu-SSZ-13 and Cu-SAPO-34 have similar crystallinity framework, chabazite (CHA). The structure can be identified as double six-membered rings (d6r) interconnected with four-membered rings (4r). The AABBCCAA stacking sequence of the double six-membered rings leads to a cage with 8 membered ring windows [13,35,36]. The structure is shown in Fig. 1.5 [36].

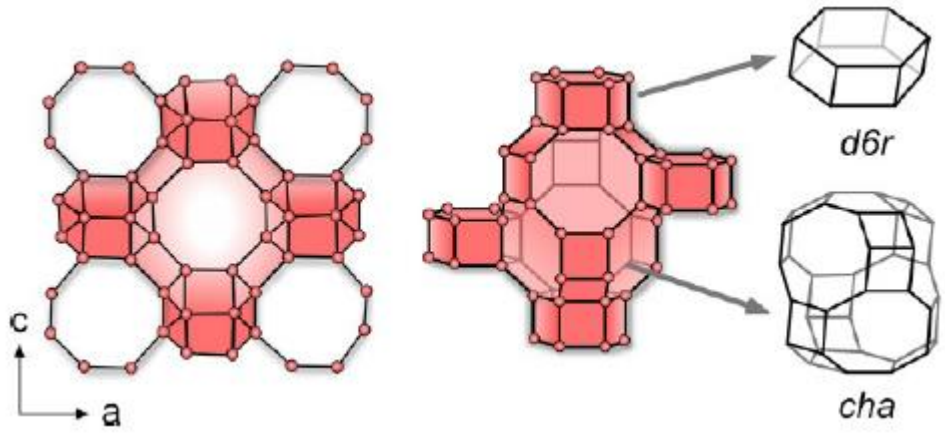


Fig. 1.5. CHA type crystal topology [36].

The difference between Cu-SSZ-13 and Cu-SAPO-34 is the composition of the structures. Cu-SSZ-13 primarily contains silicon dioxide ($SiO_2$) and a various amount of Al substitution of Si, depending on its Si/Al ratio, whereas Cu-SAPO-34 contains mainly $AlPO_4$ with various amount of Si substitution into $AlPO_4$ structure [29,37].

### 1.6 Cu active sites on Cu-CHA

Based on the X-ray diffraction (XRD) data on Cu-SSZ-13, Fickel et al. found that $Cu^{2+}$ ions are located at the double six-membered ring [38]. Two different Cu active sites were then proposed by Kwak et al. Based on their XRD and DRIFTS results, they found that Cu distribution was dependent on the Cu ion-exchange level. Cu primarily filled in the six-membered ring when the ion-exchanged level was low. When the ion-exchanged level was high enough, Cu started to fill in the eight-membered ring [39]. More studies later found out that Cu speciation does not only

depend on the ion-exchange level, but also depends on the Si/Al ratio. Giordanino et al. proposed $[Cu\text{-}OH]^+$ species by probing oxidized Cu-SSZ-13 at low temperature (100 K) with CO [40]. Anderson et al. studied the location of $Cu^{2+}$ by XRD. They further suggested that the $[CuOH]^+$ species is stable at the eight-membered ring [41]. After these studies, Z2Cu and ZCuOH were then used to identify $Cu^{2+}$ at six-membered rings and eight-membered rings, respectively, where Z denotes an Al site.

### 1.6 $NH_3$-SCR mechanism on Cu-CHA

The $NO_x$ conversion profile during steady state SCR, figure shown in Fig. 1.6, shows there is a non-monotonic profile, defined by two different temperature regions, when the Cu loading is considered low [25]. This shows that the SCR mechanism might be dependent on the temperature region.

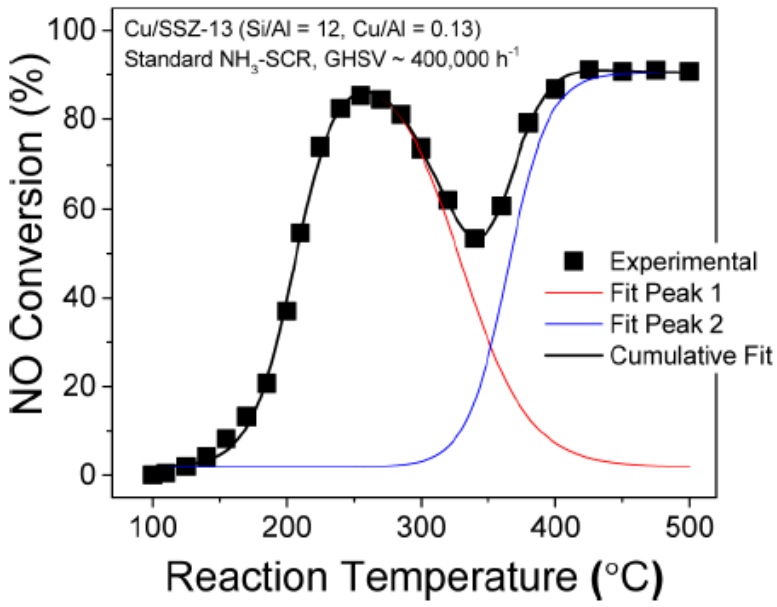


Fig. 1.6. Standard SCR performance over a Cu-SSZ-13 catalyst with Si/Al = 12 and Cu/Al = 0.13. Reactant feed contains 350 ppm NO, 350 ppm $NH_3$, 14% $O_2$, and 2.5% $H_2O$ balanced with $N_2$ at a gas hourly space velocity (GHSV) of 400,000 $h^{-1}$ [25].

Most research has been regarding the low-temperature SCR mechanism. With kinetic measurements, Gao et al. found that the SCR rate as a function of Cu loading on the catalyst is second order when the Cu loading is low. This suggests that the low-temperature SCR reactions are catalyzed by transient Cu dimers [25]. Paolucci et al. did a SCR reactant cut-off experiment and showed that NO together with $NH_3$ can effectively reduce $Cu^{II}$ to $Cu^{I}$ [31]. The reduced Cu site, $Cu^{I}(NH_3)_2$, was further proposed by considering the coordination number from Ab-initio molecular dynamics (AIMD) [32]. From $Cu^{II}$ reduction to $Cu^{I}$, this process is recognized as the reduction half cycle. To better understand the oxidation half cycle, second order fits from the CuI fraction calculation from X-ray absorption near-edge structure (XANES) spectra over multiple Si/Al ratio were derived. The second order relationship again suggests Cu dimers are present, in the form of $(NH_3)_2Cu^{II}$-$O_2$-$Cu^{II}(NH_3)_2$. Finally, DFT Calculations show that Cu becomes mobile after $NH_3$ solvation. $Cu^{I}(NH_3)_2$ can move a certain range to find another $Cu^{I}(NH_3)_2$ to form dimers shown above. The dimer species are recognized to be the key species for the oxidation half cycle [33]. Combined with the reduction half cycle, the catalytic cycle of low-temperature SCR was found. The figure describing the reduction half cycle and oxidation half cycle is shown in Fig. 1.7.

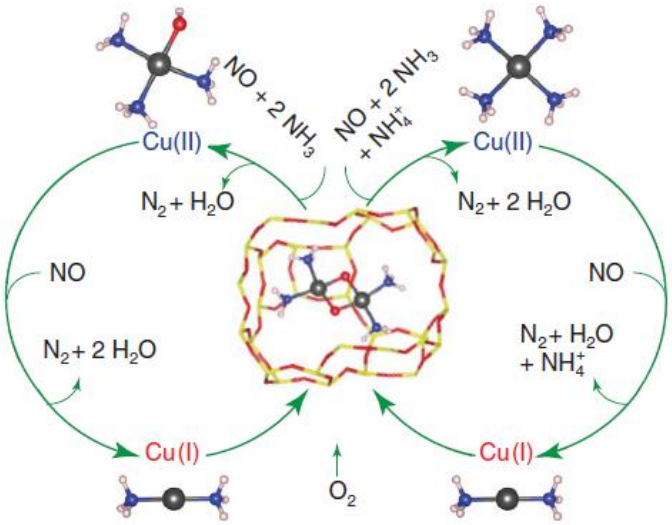


Fig. 1.7. Low-temperature SCR catalytic cycle [33].

In terms of the high-temperature SCR mechanism, fewer studies have been done, likely because of the convoluted factors at high temperatures, such as the $NH_3$ oxidation side reactin and mass transfer limitation problems [29]. Gao et al. found a linear relationship of SCR rate with respect to Cu loading when the Cu loading is low, suggesting that the monomeric Cu sites are catalyzing the SCR reactions at high temperatures [25].

### 1.7 Deactivation mechanisms of Cu-CHA

Even though the Cu-SSZ-13 catalysts are commercialized for $NO_x$ removal, they still suffer from deactivation. Among the deactivation modes, sulfur poisoning is a main one. Sulfur is common in the diesel fuel and lubricant oil. Even though ultra-low sulfur diesel fuel is mandated in the US, sulfur can still have an impact on the catalyst as accumulation of sulfur on the catalyst can deactivate the catalyst [36].

Sulfur in the exhaust can be $SO_2$ and $SO_3$. $SO_3$ comes from the oxidation of $SO_2$ on the DOC. In an early work, Cheng et al. tested the SCR performance before and after $SO_2$ or $SO_3$ exposure. They found that the low-temperature SCR performance decreased much more after the Cu-zeolite

catalyst was exposed to $SO_3$ compared to $SO_2$. Using XANES and extended X-ray absorption fine structure (EXAFS), they confirmed that Cu remained dispersed even after $SO_3$ exposure, but the formation of copper sulfate ($CuSO_4$) after $SO_3$ exposure was much more stable compared to copper sulfite (Z-$CuSO_3$) and copper hyposulfite (Z-$CuSO_2$) formed after $SO_2$ exposure. This supports the fact that $SO_3$ poisoning is more severe than $SO_2$ [42].

In most studies, sulfur decreases the catalyst low-temperature SCR activity, but has less effect on high-temperature SCR activity [4,36,42,43]. $NH_3$, a reactant in the SCR reactions, can react with sulfur species and form ammonium sulfate ($(NH_4)_2SO_4$). This species decomposes at around 350 °C [44]. This may explain why sulfur only affects the low-temperature SCR activity but not the high-temperature one. The catalyst regeneration process by $NH_3$ has been called "chemical deSOx" [4].

Multiple deactivation mechanisms related to $SO_2$ exposure have been proposed. Zeolite pore blocking caused by $SO_2$ is a common mechanism. Wijayanti et al. found the pore volume and area decreased after $SO_2$ exposure under SCR reaction conditions [45]. $(NH_4)_2SO_4$ formed by $NH_3$ and $SO_2$ is recognized as one of the pore blocking species [46]. Other mechanisms are based on the catalyst active sites that are inhibited by different sulfur species, such as $CuSO_4$, copper bisulfite ($CuHSO_3$), and $(NH_4)_2SO_4$. Based on the experiments using DRIFTS, TPD results, and DFT calculations, $SO_2$ only adsorbed on Z2Cu when cofed with $NH_3$ and formed $(NH_4)_2SO_4$. However, $SO_2$ interacts with ZCuOH readily and form $CuHSO_3$ or even $CuSO_4$ [47]. From the TPD results, $CuSO_4$ requires temperatures higher than 600 °C to decompose [48], while desorption of $(NH_4)_2SO_4$ only requires around 350 °C [47]. The results imply that catalysts with more ZCuOH lead to harder to desorb sulfur. Luo et al. confirmed this mechanism using DRIFTS with probe gas $NH_3$, showing that the T-O-T zeolite vibrational peak associated with ZCuOH disappeared, and

the vibrational peak intensity associated with Z2Cu decreased after $SO_2$ exposure [49]. Shih et al. showed that sulfur preferably stored on ZCuOH. Their computational results further showed that sulfur species can persist to higher temperature on ZCuOH than on Z2Cu, indicating that ZCuOH is more likely to remain poisoned relative to Z2Cu until higher temperatures are reached [50].

Other than sulfur poisoning, hydrothermal aging (HTA) is also considered as a deactivation mode. It can happen when the DPF periodically regenerates. The temperature of the DPF increases to burn the carbon particles when the particle loading reaches a certain limit. A large amount of heat due to C oxidation transfers to the downstream SCR catalyst. The high-temperature exposure (>650 °C) with the presence of moisture in the feed may lead to zeolite structure damage.

Many previous studies have focused on the hydrothermal stability of Cu-CHA. Fickel et al. showed that the small pores of Cu-CHA are an advantage. Since Cu-CHA has a pore size around 3.8 Å, smaller than the kinematic diameter of Al, the catalyst is less vulnerable to dealumination than other mesoporous catalysts [51]. Although the Cu-CHA catalyst is less likely to dealuminate during hydrothermal aging, it will still undergo deactivation if exposed to high temperature conditions. Schmieg et al. showed that aging temperature and aging time are important variables for hydrothermal aging. Their results showed that when the catalysts were hydrothermally aged at 3 h/900 °C, 8 h/875 °C, 12 h/850 °C, or 72 h/800 °C, the highest $NO_x$ conversion of catalysts decreased to lower than 70% [52]. The distribution of Cu sites was also found to determine the catalyst's hydrothermal stability. The Cu located in the eight-membered ring had lower hydrothermal stability. During hydrothermal aging, it aggregated and formed $CuO_x$ particles which damaged the zeolite structure [53–55]. Although the catalyst structure damage during hydrothermal aging is the usual concern, Luo et al. proposed that mild hydrothermal aging (<750 °C) did not affect the zeolite structure. Instead, the copper distribution changed, with a shift from

ZCuOH to Z2Cu sites [56]. The transformation was then proposed to change the catalyst's oxidation activity [49].

### 1.8 Research Objectives

Even though many sulfur poisoning mechanisms on Cu-SSZ-13 have been proposed, detailed studies of combined sulfur poisoning and hydrothermal aging are few. Wei et al. [57] and Xi et al. [58] both found out that sulfur poisoning extent decreased after the Cu-SSZ-13 catalyst was mildly hydrothermally aged, at temperatures below 750 °C. We explored the reason behind this, with focus on how the change in the Cu site distribution during HTA affects the extent of sulfur poisoning. Next, we focused on quantification of Cu sites before and after sulfur poisoning, especially for the static Cu dimers, as predictions by our collaborators suggest those would bind sulfur strongly. We used CO titration and diffuse reflectance ultraviolet-visible (DR UV-vis) spectra techniques to quantify and characterize the change. Finally, we were interested in the impact of hydrothermal aging with different exhaust gas components on the catalyst. Understanding what, if any, gas components affect the changes associated with hydrothermal aging is important.

# Chapter 2 How Changes in Cu-SSZ-13 Catalytic Oxidation Activity via Mild Hydrothermal Aging Influence Sulfur Poisoning Extents

This chapter was reproduced with permission from the Royal Society of Chemistry. It has been published and can be found in Chen et al., ***Catal. Sci. Technol.***, 2022, **12**, 6891-6902. The introduction may be redundant with the Introduction section in the thesis, but for completeness, it is still presented here. The supplementary materials for this paper/chapter are in appendix A. The reference numbers were relabeled to be consistent in the thesis.

## 2.1 Abstract

Cu-SSZ-13 is widely used as a $NO_x$ reduction catalyst in diesel engine after-treatment systems. However, sulfur, a common although trace component in diesel fuel, can lead to catalyst deactivation. Literature has shown that the relative amounts of Cu sites identified as Z2Cu and ZCuOH under inert conditions lead to different S poisoning extents and those relative Cu site amounts can be influenced by mild hydrothermal aging. Our results confirm this finding, but only for specific conditions, in other words the different Cu distributions leading to different extents of S poisoning is not universally true. Here, we show that the extent of sulfur poisoning by $SO_2$ in the absence of water is related to $SO_2$ oxidation on the Cu sites, and more specifically the ZCuOH sites. Therefore, since different pretreatment conditions lead to different relative ZCuOH and Z2Cu distributions, the extent of $SO_2$ oxidation and therefore S poisoning is influenced by these different pretreatment conditions. The catalyst with more ZCuOH had higher $SO_2$ oxidation conversions and more deactivation compared to a catalyst with less relative ZCuOH. However, if $SO_3$ was included during sulfur exposures or if the experiment was performed at relatively low temperature with an $SO_2$ exposure, changes in the Cu distribution made less or no difference. This is correlated to S oxidation extents. In the presence of water, the extent of sulfur poisoning is also

affected by the catalyst's ability to oxidize $SO_2$. And, the presence of water leads to further deactivation than in its absence. The water effect is apparent when the oxidation activity is relatively weak and is less significant when the $SO_2$ oxidation extent is relatively strong.

## 2.2 Introduction

Selective catalytic reduction (SCR) of $NO_x$ by $NH_3$ over metal-exchanged zeolites is a common approach to eliminate nitrogen oxides ($NO_x$) from diesel engine exhaust. Among metal exchanged zeolite-based catalysts, Fe- and Cu-exchanged zeolites appear to be the most commonly studied [17-34]. And among Cu-zeolite catalysts studied, the Cu-SSZ-13 formulation has received significant attention as it is reported to be less prone to hydrothermal degradation compared to Cu-ZSM-5, Cu-beta, and Cu-Y and its small pores makes it more resistant to hydrocarbon poisoning than other mesoporous catalysts [16,51,59,60].

Although Cu-SSZ-13 is commercially used as an SCR catalyst to reduce NO to $N_2$ in diesel engine exhaust [56,61–65], it is still susceptible to sulfur poisoning. Using temperature programmed desorption (TPD) experiments, Su et al. proposed that several sulfur species form on Cu-SSZ-13 catalysts with sulfur exposure, including $H_2SO_4$, $CuSO_4$, and $Al_2(SO_4)_3$ [48]. When $NH_3$ is included during a sulfur exposure, $(NH_4)_2SO_4$ like species are also observed [44,46,66,67].

The impact of $SO_2$ and $SO_3$ on SCR activity has mainly been observed or studied at temperatures below 350 °C [42,68]. Research has shown that the activity can be recovered by high temperature treatment, for example at temperatures over 550 °C [4,36]. Kumar et al. showed that by including $NH_3$ or $C_3H_6$ in the regeneration mixture, which the authors termed chemical de$SO_x$, sulfur was released from the catalyst at a lower temperature, around 400 °C [4]. Jangjou et al. further showed that ammonium sulfate species, formed on SCR catalysts during exposure to $SO_2$

in the presence of $NH_3$, decomposed at around 350 °C [44,66]. This may explain why decreased SCR activity has primarily been observed in the low-temperature region, because $NH_3$, a reactant in the SCR reaction, leads to formation of ammonium sulfate, which decomposes at temperatures higher than 350 °C, allowing activity to be regenerated.

Multiple deactivation mechanisms associated with $SO_2$ exposure have been proposed. A common one is pore blocking by sulfur containing species. Zhang et al. used $NH_3$ TPD to characterize a catalyst and proposed that after $NH_3$ and $SO_2$ exposure, $(NH_4)_2SO_4$ species formed and might poison the active sites and block catalyst pores [46]. Wijayanti et al. found the catalyst surface area and pore volume decreased after $SO_2$ exposure under SCR reaction conditions [45]. Other proposed sulfur poisoning mechanisms include $SO_2$ interacting with different Cu sites. Z2Cu and ZCuOH have been identified as two ion-exchanged Cu species on the catalyst (where Z denotes an isolated Al site) under inert conditions [39,55,56,69–72] and recent research has found that different sulfur species form on these two Cu site types after sulfur exposure. For example, it has been proposed that $CuSO_4$ or $CuHSO_4$ forms on ZCuOH while $(NH_4)_2SO_4$ forms on Z2Cu [44]. Luo et al. studied a SCR catalyst using diffuse reflectance infrared Fourier transform spectroscopy (DRIFTS) during $NH_3$ adsorption and showed the loss of a T-O-T zeolite vibration feature associated with ZCuOH after sulfur exposure, suggesting that $NH_3$ no longer interacted with ZCuOH [49]. Shih et al. showed that sulfur stored preferably on ZCuOH compared to Z2Cu. Their computational results further showed that sulfur species persist to higher temperature on ZCuOH than Z2Cu, indicating that ZCuOH is more likely to remain poisoned relative to Z2Cu until higher temperatures are reached [50].

Based on these findings, one approach proposed to protect a Cu-SSZ-13 catalyst from sulfur poisoning is to decrease the amount of ZCuOH in favor of more Z2Cu sites. It has been shown

that ZCuOH can be transformed to Z2Cu by mild hydrothermal aging without zeolite damage, using hydrothermal aging conditions at temperatures below 750 °C [52,56,72]. Wei et al. showed that the extent of $SO_2$ poisoning decreased after a 750 °C pretreatment [73]. Xi et al. found that increasing the mild hydrothermal aging duration at 650 °C prior to $SO_2$ and $SO_3$ exposure under SCR reaction conditions reduced the impact of sulfur on SCR activity [58].

We observed similar trends, with mild hydrothermal aging decreasing the extent of $SO_2$ poisoning when $SO_2$ was used as the sulfur species in a 400 °C exposure. However, with $SO_3$ poisoning, the mild hydrothermal aging treatment *did not* mitigate the impact of poisoning on SCR activity. We used in situ DRIFTS to identify the relationship between the oxidation activity and the amount of ZCuOH, and these combined with SCR and oxidation reaction results show a relationship between the catalytic oxidation activity and the extent of sulfur poisoning whether in the presence or absence of water. We here propose that the extent of sulfur poisoning is dependent on the extent of $SO_2$ oxidation on the catalyst surface, which in itself is a function of the relative amounts of ZCuOH and Z2Cu, further clarifying differences observed with different Cu type distributions and differences in our observations and those in the literature.

### 2.3 Experimental Methods

The Cu-SSZ-13 catalyst was provided by Cummins Inc. and came as a honeycomb monolith structure with a cell density of 300 cells/in$^2$ (cpsi). Cylindrical samples were core drilled from the monolith and were 2.9 cm in length with a diameter set such that each had 21 cells. The catalyst was wrapped with ceramic fiber strings and placed in a quartz tube, purchased from Quartz Scientific, which was placed in a Lindberg Blue M Mini-Mite tube furnace. Two K-type Omega thermocouples placed in the upstream and downstream radial center of the monolith were used to measure the catalyst temperature.

Sulfinert coated tubing and fittings from Swagelok were used upstream and downstream of the quartz tube reactor. Upstream and downstream tubing were heated to 150 °C using heat tape and wrapped in insulation to prevent $H_2O$ condensation on the tubing surface. All gases, except some of the $N_2$ used as a carrier for the steam, were metered using MKS Instruments mass flow controllers. A $N_2$ generator purchased from Parker Balston was used to supply some of the balance $N_2$ and all other gases originated from cylinders purchased from Praxair or Matheson. Steam was introduced using a Bronkhorst controlled evaporator mixer. CO, $CO_2$, $H_2O$, NO, $NO_2$, $N_2O$, $NH_3$, $SO_2$, $SO_3$, and $H_2SO_4$ reactor outlet concentrations were measured using a MKS MultiGas 2030 FT-IR.

For the reactor experiments, a total flow rate of 1360 sccm was used, which corresponds to a GHSV of 62300 $h^{-1}$. The monolith-supported catalysts were either "degreened" or exposed to mild hydrothermal aging conditions, hereafter denoted HTA, prior to experiments. For degreening, the catalyst sample was exposed to 10% $O_2$, 7% $H_2O$, 8% $CO_2$ and balance $N_2$ at 550 °C for 4 h, while the mild HTA was done with the same gas concentrations but at 600 °C for 10 or 25 h. The results obtained for the 25 h sample are used throughout the paper, and the results from the 10 h sample are included in the Supporting Information. $SO_2$ exposure was conducted at 200 or 400 °C with 50 ppm $SO_2$, 10% or 1% $O_2$, 0, 0.5% or 7% $H_2O$ and balance $N_2$. $SO_3$ exposure was conducted at 200 °C with 25 ppm $SO_2$, 25 ppm $SO_3$, 10% $O_2$ and balance $N_2$. The mild HTA temperature used and S exposures, based on prior literature, should not lead to any changes in zeolite crystallinity or structure [56,58,62,63,68]. Before an experiment, the catalyst was exposed to 10% $O_2$ and balance $N_2$ at 500 °C for 1 h, except for the experiments after the catalyst was exposed to sulfur. After the $O_2$ exposure pretreatment, the temperature was cooled to 150, 200, or 400 °C depending on the experiment to be run. Catalyst performance test conditions are listed in Table 2.1.

Table 2.1 Reaction conditions used

| Reactions | $NH_3$ (ppm) | NO (ppm) | CO (ppm) | $SO_2$ (ppm) | $H_2O$ (%) | $CO_2$ (%) | $O_2$ (%) | $N_2$ |
|---|---|---|---|---|---|---|---|---|
| SCR | 200 | 200 | - | - | 7 | 8 | 10 | Balance |
| NO oxidation | - | 200 | - | - | 7 | 8 | 10 | Balance |
| $NH_3$ oxidation | 200 | - | - | - | 7 | 8 | 10 | Balance |
| CO oxidation | - | - | 200 | - | 7 | - | 10 | Balance |
| $SO_2$ oxidation | - | - | - | 50 | - | - | 10 | Balance |

Calculations include:

$NO_x$ conversion during SCR reaction = $\frac{NO_{x_{in}} - NO_{x_{out}}}{NO_{x_{in}}} \times 100\%$ (2-1)

NO oxidation conversion = $\frac{NO_{in} - NO_{out}}{NO_{in}} \times 100\%$ (2-2)

$NH_3$ oxidation conversion = $\frac{NH_{3_{in}} - NH_{3_{out}}}{NH_{3_{in}}} \times 100\%$ (2-3)

CO oxidation conversion = $\frac{CO_{in} - CO_{out}}{CO_{in}} \times 100\%$ (2-4)

$SO_2$ oxidation conversion = $\frac{SO_{2_{in}} - SO_{2_{out}}}{SO_{2_{in}}} \times 100\%$ (2-5)

Diffuse reflectance infrared Fourier transform spectroscopy (DRIFTS) during $NH_3$ adsorption was used to characterize the degreened and HTA catalysts T-O-T vibration region. We used a

Nicolet iS-50 FT-IR spectrometer with a Harrick Scientific Praying Mantis cell and ZnSe windows. Catalyst powder was scraped from the commercial monolith-supported catalysts. These were filled into a sample cup and the sample surface was leveled to the cup height. A mixture of dry ice and isopropanol was used as a cold trap to remove residual water from the inlet line into the cell. The total flow rate for all experiments and treatments was 50 sccm. Before experiments, catalysts were exposed to 10% $O_2$ and balance He at 500 °C for 1 h ($O_2$ pretreatment). Then, the system was cooled down to the experiment temperature. The background spectrum was taken after the catalyst had cooled to the target temperature. For $NH_3$ adsorption experiments, the experiments were conducted at 120 °C with 1000 ppm $NH_3$ and balance He.

$NH_3$ temperature programmed desorption (TPD) and $NH_3$ temperature programmed oxidation (TPO) experiments were also conducted. From these, for example, we determined the temperature for the onset of $NH_3$ oxidation temperature in the DRIFTS cell, ~300 °C. The $NH_3$ oxidation experiments and experiments with $NH_3$ exposure followed by a He purge at that temperature were used to characterize the relationship between ZCuOH and the $NH_3$ oxidation activity of the catalyst. For $NH_3$-TPD and TPO experiments, background spectra were taken and recorded every 10 °C during the cool down phase after the pretreatment, to 120 °C. After $NH_3$ adsorption, $NH_3$ was turned off and there was a He purge for 30 min before the TPD phase. For the TPO experiments, 10% $O_2$ was introduced after $NH_3$ was turned off. Then, the temperature was ramped to 500 °C at 10 °C/min. During the temperature ramp, spectra were taken every 10 °C. The background spectrum for each temperature was subsequently subtracted from each spectrum at its corresponding temperature. For the isothermal $NH_3$ oxidation and He purge experiments at 300 °C, after a 10% $O_2$ in He pretreatment at 500 °C for 1 h, the temperature was cooled to 300 °C. After a background spectrum was taken, $O_2$ was turned off and 1000 ppm $NH_3$ in He was

introduced for 1 h. Then, 10% $O_2$ was introduced for the $NH_3$ oxidation experiment, or only He when doing the He purge experiment. We note that $NH_3$ TPD experiments are often used to characterize SCR catalyst acidity, but after S exposures the formation of ammonium sulfates convolute any interpretation [43,44,49].

## 2.4 Results and Discussion

*Catalyst $NH_3$-SCR and CO, NO, $NH_3$ and $SO_2$ oxidation performance before sulfur exposure*

Before sulfur exposure, SCR and NO, CO, $NH_3$ and $SO_2$ oxidation experiments were conducted using the degreened and HTA catalyst samples. The SCR results are shown in Fig. 2.1 (a). Below 350 °C, similar SCR conversions were obtained over both catalysts. These results are consistent with other literature results that show similar SCR conversions if the catalysts were pretreated below 700 °C [49,52,62,63,74]. Above 350 °C, the HTA catalyst resulted in higher $NO_x$ conversions compared to the degreened catalyst. SCR reactions at high temperatures are affected by $NH_3$ oxidation, where a loss in $NH_3$ through oxidation by $O_2$ instead of NO can lead to a decrease in $NO_x$ conversion [17,49,63]. The higher $NO_x$ conversion attained over the HTA catalyst is explained by lower $NH_3$ oxidation conversion, as is confirmed in Fig. 2.1 (b). Not only does $NH_3$ oxidation conversion decrease after HTA, but NO to $NO_2$, CO to $CO_2$, and $SO_2$ to $SO_3$ oxidation conversions also decrease, as shown in Fig. 2.1 (c), (d), and (e). These results demonstrate there is a consistent loss in oxidation reaction conversion, at least for these four reactants, due to the HTA pretreatment. This is somewhat consistent with Luo et al.'s work where although they used higher temperatures for hydrothermal aging, it was shown that NO and $NH_3$ oxidation conversions decreased after 700 and 800 °C compared to 550 °C aging exposures [49].

As a note, in terms of $N_2O$ formation, as shown in the Appendix A, Fig. A-1, the amount of $N_2O$ formation over both catalysts was similar. $N_2O$ formation follows the pattern typically observed in other literature studies, with a low temperature peak via ammonium nitrate decomposition and a high temperature peak associated with $N_2O$ formed during $NH_3$ oxidation [14,75]. In terms of how the aging affects $N_2O$ formation, our results do not parallel those in the literature [73] where different relative amounts of $N_2O$ formed in the low temperature regime with changes in hydrothermal aging temperature. A likely explanation for this discrepancy is the different experimental and aging conditions. There is a larger difference between the "degreened" and HTA samples in the literature cited compared to those we used. In general, the amount of $N_2O$ formed was low as is consistent with literature for this Cu-SSZ-13 catalyst. As no $NO_2$ was formed, $N_2$ selectivity can be calculated based on NO conversion and $N_2O$ formed.

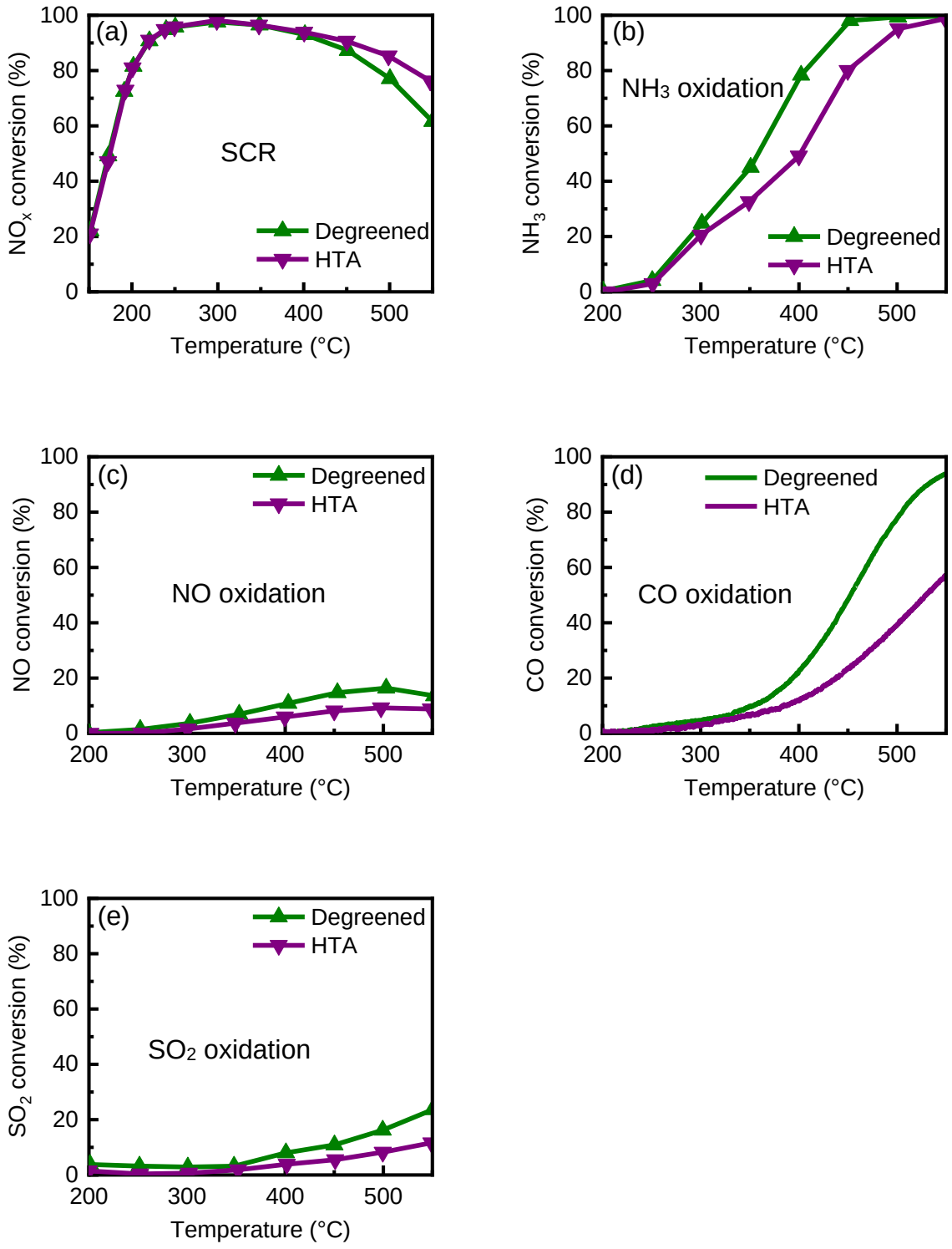


Fig. 2.1. (a) $NH_3$-SCR and (b) $NH_3$, (c) NO, (d) CO, and (e) $SO_2$ oxidation for the degreened and HTA catalysts before sulfur exposure. Reaction conditions are described in Table 2.1.

Evidence in the literature shows a relationship between NO and $NH_3$ oxidation and ZCuOH amount [17,49,76]. To further support the relationship between the oxidation activity and the amount of ZCuOH, we used in-situ DRIFTS to characterize the sample during $NH_3$ oxidation experiments at 300 °C, see Fig. 2.2 (a). Note, other techniques are sometimes used to quantify Cu site distributions, such as $H_2$ temperature programmed reduction ($H_2$-TPR) [39,44,56,77]. However, the sample used here is a commercial sample, with an unknown initial amount of Cu/CuO particles. The reduction of CuO particles occurs at a similar temperature as ZCuOH, which could therefore complicate any quantification analysis [18]. Furthermore, relative amounts of Z2Cu and ZCuOH are sufficient to explain the findings and conclusions, as demonstrated below. In the DRIFTS results used here, the T-O-T vibration region is shown, where the 900 $cm^{-1}$ peak has been assigned to $NH_3$ interacting with Z2Cu and the 950 $cm^{-1}$ peak has been assigned to ZCuOH [39,44,56,63]. The $NH_3$ oxidation temperature was determined from $NH_3$ TPD and $NH_3$ TPO experiments using separate DRIFTS experiments, see Appendix A, Fig A2. From 120 to 300 °C during both the TPD and TPO experiments, the intensities of both the 900 and 950 $cm^{-1}$ features decrease at similar rates. Above 300 °C, however, both the 900 and 950 $cm^{-1}$ peaks diminished much faster during the TPO experiment compared to those peaks during the TPD experiment. These results suggest that below 300 °C, $NH_3$ desorption from both ZCuOH and Z2Cu occurred, while above 300 °C, $NH_3$ oxidation started to be significant. With this observation, 300 °C was chosen as a temperature to compare $NH_3$ oxidation characteristics. In Fig. 2 (a), the intensities of both the 900 and 950 $cm^{-1}$ decreased during $NH_3$ oxidation at 300 °C. The 950 $cm^{-1}$ feature, in particular, decreased more than 900 $cm^{-1}$ feature, suggesting that $NH_3$ on ZCuOH was oxidized more rapidly than on Z2Cu. To rule out the possibility that $NH_3$ desorption at 300 °C is significant compared to the oxidation, the $NH_3$ adsorption and then He purge at 300 °C experiment was

conducted, with results shown in Fig. 2.2 (b). Compared to $NH_3$ oxidation, $NH_3$ desorbed much slower from both ZCuOH and Z2Cu, corroborating that the decrease in the intensities of both peaks in Fig. 2.2 (b) was not because of $NH_3$ desorption, but stems from $NH_3$ oxidation. And, these results are also consistent with the observations in Figure 2.1 (a) and 2.1 (b).

ZCuOH has been hypothesized to be the more active $NH_3$ oxidation active site [17,49,76]. Literature [56,61,62,78] and our results show that during mild hydrothermal aging, Cu can migrate from ZCuOH to Z2Cu sites. For example, as shown in Figure A3 (a) in the Appendix A, the intensity of the 950 $cm^{-1}$ peak, after normalizing the 900 $cm^{-1}$ intensities, for the degreened catalyst is greater than that for the HTA sample. This suggests a loss in ZCuOH, with an increase in Z2Cu after a mild HTA treatment. Furthermore, this migration of Cu from ZCuOH to Z2Cu results in the loss of Brønsted acid sites. In the DRIFTS results shown in Appendix A, Figure A3 (b), the 1620 $cm^{-1}$ peak, representing $NH_3$ adsorption on Lewis acid sites [49,79,80], is normalized in order to compare its intensity with the intensity of 1460 $cm^{-1}$ peak, representing $NH_3$ adsorption on Brønsted acid sites [49,79,80]. The results show that after HTA, there are fewer Brønsted acid sites, suggesting that the Brønsted acid sites are consumed during HTA. In summary, the results suggest that the degreened sample has more ZCuOH than the HTA sample and explains why the degreened sample has higher $NH_3$ oxidation conversions than the HTA samples at temperatures above 300 °C, shown in Fig. 2.1 (b), further supported by the DRIFTS results in Fig 2.2 (a).

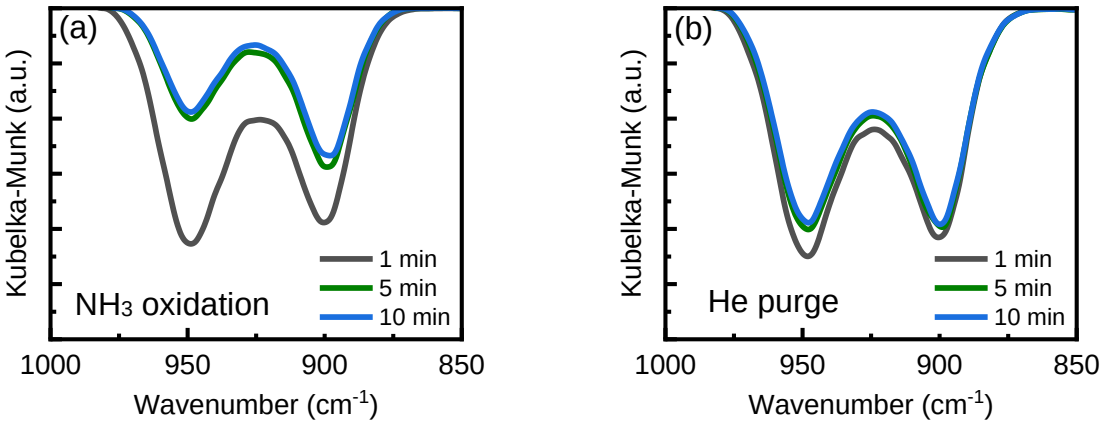


Fig. 2.2. DRIFTS spectra of (a) $NH_3$ oxidation and (b) He purge at 300 °C after 10% $O_2$ pretreatment at 500 °C for 1 h and 1000 ppm $NH_3$ adsorption at 300 °C for 1 h.

*How catalyst surface $SO_2$ oxidation activity impacts $SO_2$ poisoning*

Based on literature results, ZCuOH has been proposed to accumulate more sulfur than Z2Cu at 200 °C (0.6 S/Cu vs. 0.3 S/Cu) [50]. In addition, the sulfur species on ZCuOH require higher temperatures to decompose compared to sulfur species on Z2Cu [44,50], so reducing the amount of ZCuOH in the catalyst has been proposed to reduce the extent of sulfur poisoning [58,73]. We first exposed both the degreened and HTA catalysts to $SO_2$ at 400 °C and $NO_x$ conversions during subsequent SCR reaction experiments were evaluated, with results from before and after $SO_2$ exposure shown in Fig. 3. The results show that after $SO_2$ exposure, the degreened catalyst led to lower $NO_x$ conversions from 150 to 300 °C compared to the HTA catalyst, suggesting that the hydrothermal aging treatment indeed helped reduce the extent of sulfur poisoning as has been previously suggested.

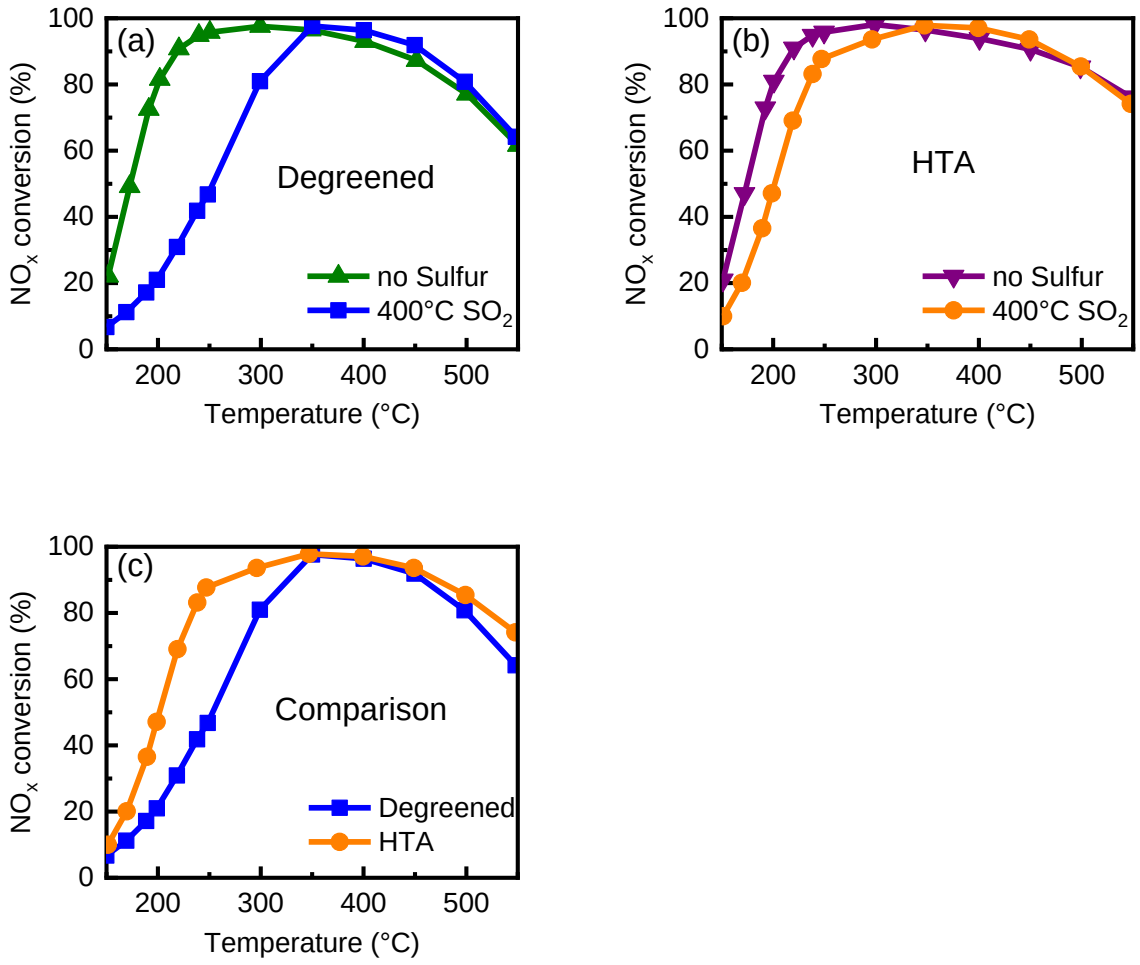


Fig. 2.3. SCR results after 50 ppm $SO_2$ exposure at 400 °C on (a) degreened and (b) HTA catalysts. The comparison between SCR conversion after $SO_2$ exposure at 400 °C on degreened and HTA catalysts is in (c). The SCR reaction conditions are described in Table 2.1.

As an aside, an interesting finding from the results in Fig. 3 (a) and (b) is that both catalysts resulted in higher $NO_x$ conversions during SCR above 350 °C after $SO_2$ exposure relative to the samples not exposed to $SO_2$. A possible explanation is that $NH_3$ oxidation was inhibited by $SO_2$. If so, since NO conversions under SCR conditions at high temperatures can be lower due to loss of reactant $NH_3$ by $NH_3$ oxidation, $NH_3$ oxidation inhibition could lead to higher $NO_x$ conversions. To test the $NH_3$ oxidation inhibition by $SO_2$ hypothesis, we did an $NH_3$ oxidation experiment after

400 °C $SO_2$ exposure, see Appendix A, Fig. A4. The results show that the $NH_3$ oxidation was inhibited below 500 °C compared to the $NH_3$ oxidation results using the catalyst prior to $SO_2$ exposure. This $NH_3$ oxidation inhibition by $SO_2$ might explain the increased $NO_x$ conversion during SCR between 350 and 450 °C after $SO_2$ exposure.

After exposure to a mixture containing $SO_3$, both the degreened and HTA catalysts were significantly deactivated below 350 °C, see Fig. 2.4, and that loss led to similar $NO_x$ conversions over both samples in this lower temperature range, see Appendix A, Fig. A5 (a) for a direct comparison. Contrary to the results shown above and the associated literature discussed, here the hydrothermal aging treatment did not mitigate the extent of $SO_3$ poisoning. Literature has consistently shown that $SO_3$ leads to a higher level of SCR catalyst deactivation compared to $SO_2$ [36,42,81], with one explanation being higher levels of copper sulfate formation [42]. Our results show a similar trend in that the extent of $SO_3$ poisoning is higher compared to $SO_2$ poisoning, see Fig. 2.4 (a) and (c) for the degreened catalyst and Fig. 2.4 (b) and (d) for the HTA catalyst. Furthermore, after the catalysts were exposed to $SO_2$ at 200 °C in the absence of $SO_3$, see Fig. 2.4 (c) and (d), both degreened and HTA catalysts had similar $NO_x$ conversions below 350 °C. Even though the degreened catalyst had slightly lower $NO_x$ conversions below 350 °C after $SO_2$ exposure compared to the $NO_x$ conversions of the HTA catalyst, for a direct comparison, see Appendix A, Fig A5 (b), the difference is relatively small. From these two sets of experimental results, reducing the amount of ZCuOH by using a mild hydrothermal aging treatment does not effectively protect the catalyst from $SO_2$ or $SO_3$ poisoning at 200 °C, but does for $SO_2$ exposure at 400 °C. The 400 °C results are consistent with prior work by Xi et al [58], but here the additional data at 200 °C show that the transformation of ZCuOH to Z2Cu unfortunately does not universally lead to enhanced sulfur poisoning resistance.

To resolve the seemingly contradictory results in Figures 2.3 and 2.4, and with aspects of prior literature, we propose that SCR catalyst deactivation via sulfur poisoning has some dependence on $SO_2$ oxidation activity over the catalyst surface. For the exposures that include $SO_3$, $SO_3$ being the product of $SO_2$ oxidation, there is no observed difference in the loss in $NO_x$ conversion over the two catalysts. The HTA catalyst shows similar SCR conversions below 350 °C when compared to the degreened catalyst. In terms of the SCR activity after the 200 °C $SO_2$ exposure, both degreened and HTA catalysts have poor $SO_2$ oxidation at 200 °C, see Fig. 2.1 (e) as a surrogate to support this assumption, so again they appear to respond similarly. Furthermore, neither was significantly deactivated. Therefore, under conditions where there is not significant $SO_2$ oxidation activity or the oxidation product is included in the reactant gas mixture, the two catalysts respond similarly.

However, this is not the case when experiments were run with $SO_2$ in the absence of $SO_3$ at the higher temperatures, where there would be an increase in the extent of $SO_2$ oxidation. Results from the experiments where the samples were exposed to $SO_2$ at 200 or 400 °C are shown in Figures 2.3 and 2.4 with the overlaid comparisons shown in Appendix A, Fig. A6 (a) and (b). Both the degreened and HTA catalysts after 400 °C $SO_2$ exposure were deactivated more than after the 200 °C $SO_2$ exposure. We relate this to $SO_2$ oxidation extent on the catalyst surface, with higher levels of oxidation at the higher temperature.

The hypothesis was further tested by evaluating SCR of $NO_x$ conversions after $SO_2$ exposure at 400 °C but with a lower $O_2$ concentration, 1%, during the $SO_2$ exposure, see Fig. 2.5 (a). The results show that $SO_2$ exposure with 10% $O_2$ deactivated the catalyst more than with 1% $O_2$. As an ancillary test of oxidation activity, $NH_3$ oxidation was also evaluated, see Fig. 2.5 (b). The results show that with 10% $O_2$, higher $NH_3$ oxidation conversions are also attained relative to those

with 1% $O_2$. These results are consistent with higher oxidation activities leading to more significant sulfur-derived SCR catalyst deactivation.

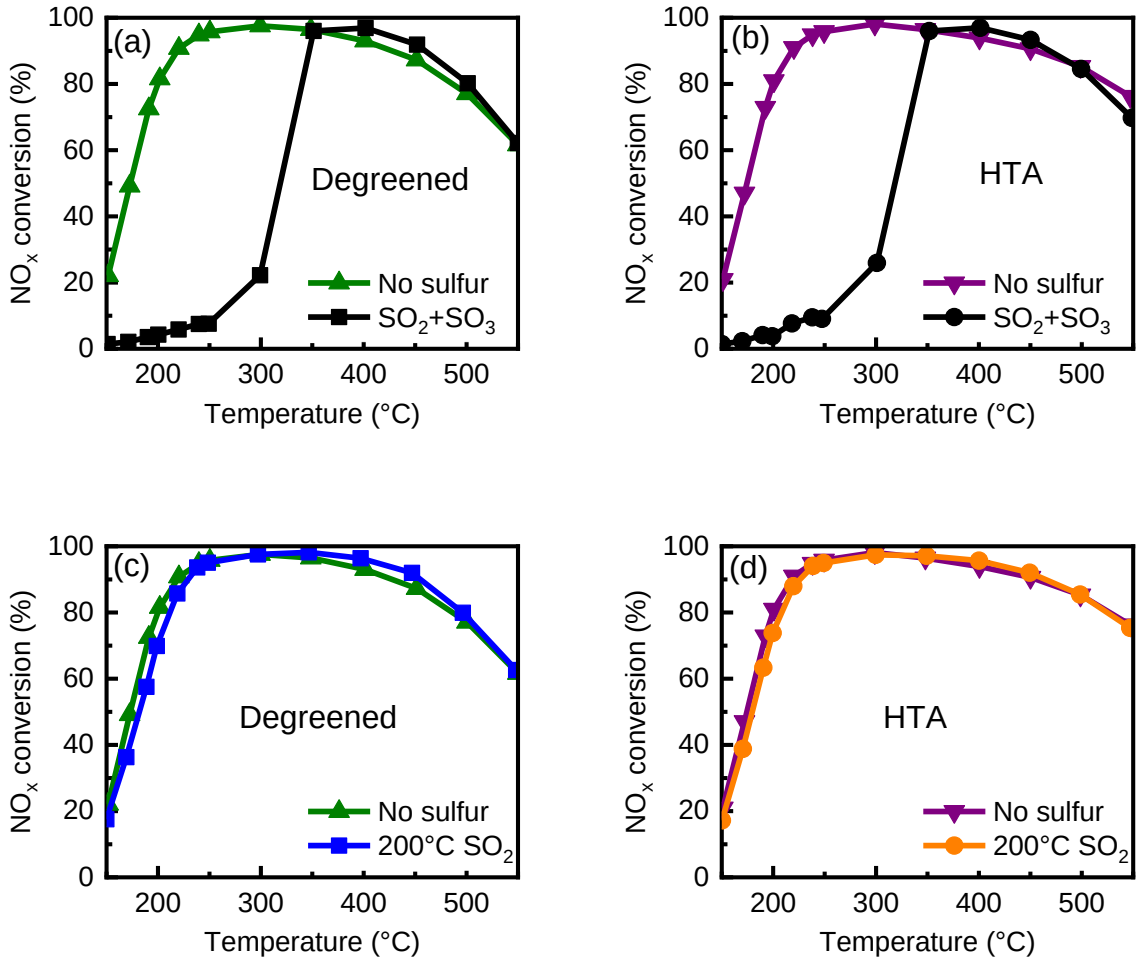


Fig. 2.4. SCR results after 25 ppm $SO_2$ and 25 ppm $SO_3$ exposure at 200 °C for 6.5 h, (a) and (b), and 50 ppm $SO_2$ exposure at 200 °C for 6.5 h, (c) and (d), on degreened, (a) and (c), and HTA, (b) and (d), catalysts. The SCR reaction conditions are described in Table 2.1.

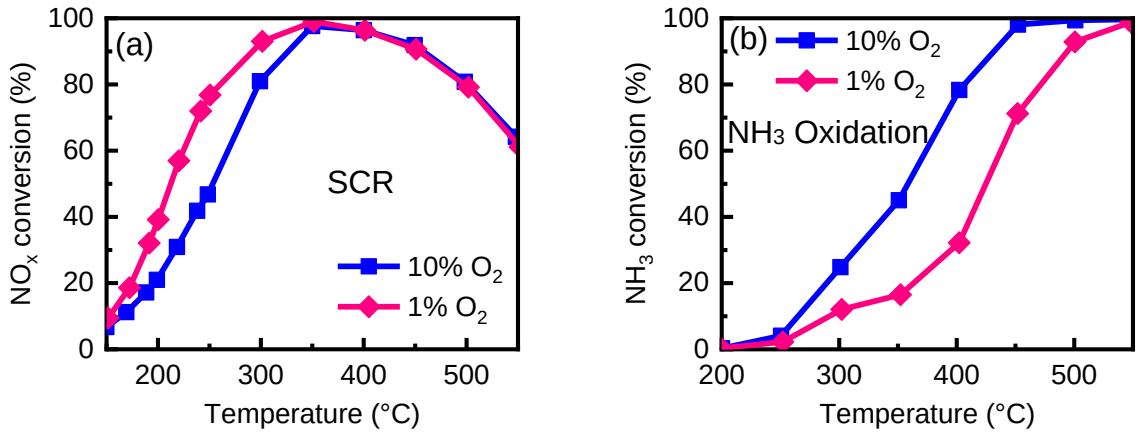


Fig. 2.5. (a) SCR results after 50 ppm $SO_2$ exposure at 400 °C for 6.5 h with 10 and 1% $O_2$ on degreened catalysts. (b) $NH_3$ oxidation results with 10 and 1% $O_2$ on degreened catalysts. Reaction conditions are shown in Table 2.1.

*How catalyst surface $SO_2$ oxidation activity impacts $SO_2$ poisoning in the presence of water*

The results above show the SCR of $NO_x$ conversions change after sulfur exposure in the absence of water (dry). However, the effect of water needs to be considered as it is a primary component of engine exhaust and is known to affect oxidation reactions among others.

We first tested whether catalyst deactivation with exposure to $SO_2$ still showed a dependency on $SO_2$ oxidation activity in the presence of water. We compared SCR results of the degreened and HTA catalysts after $SO_2$ exposure in the presence of water at 200 and 400 °C, with NO conversion results shown in Fig. 2.6. Similar to the trend with $SO_2$ exposure under dry conditions at 200 °C, both catalysts had similar $NO_x$ conversions below 350 °C after $SO_2$ exposure in the presence of water at 200 °C. And again, the SCR performance after $SO_2$ exposure at 400 °C in the presence of water led to different $NO_x$ conversions between the two catalysts, see Fig. 2.6 (b). The degreened catalyst led to lower $NO_x$ conversions below 350 °C than the HTA catalyst, again which

we attribute to the degreened catalyst having a higher $SO_2$ oxidation activity. These trends are consistent with those observed under dry conditions.

SCR experiments after a HTA pretreatment for 10 h and after this pretreatment and a sulfur exposure in the presence of water have also been conducted. The SCR comparison results are shown in the Appendix A, Fig. A7 (a) and (b). $NO_x$ conversions below 350 °C are similar no matter what pretreatment conditions after the 200 °C $SO_2$+$H_2O$ exposure, with results shown in Appendix A, Fig A7 (a), but 25 h HTA > 10 h HTA > degreened after 400 °C $SO_2$+$H_2O$ exposure, with results shown in Fig A7 (b). These results again can be attributed to the catalyst surface $SO_2$ oxidation activity difference during $SO_2$ exposure. At 200 °C, poor oxidation activity is observed for all three catalysts. However, at 400 °C, the oxidation activity of the degreened catalyst is higher than that of the 10 h HTA catalyst, which is higher than that of the HTA catalyst aged for 25 h. $NH_3$ oxidation activity results were also obtained and are shown in Appendix A, Fig. A7 (c).

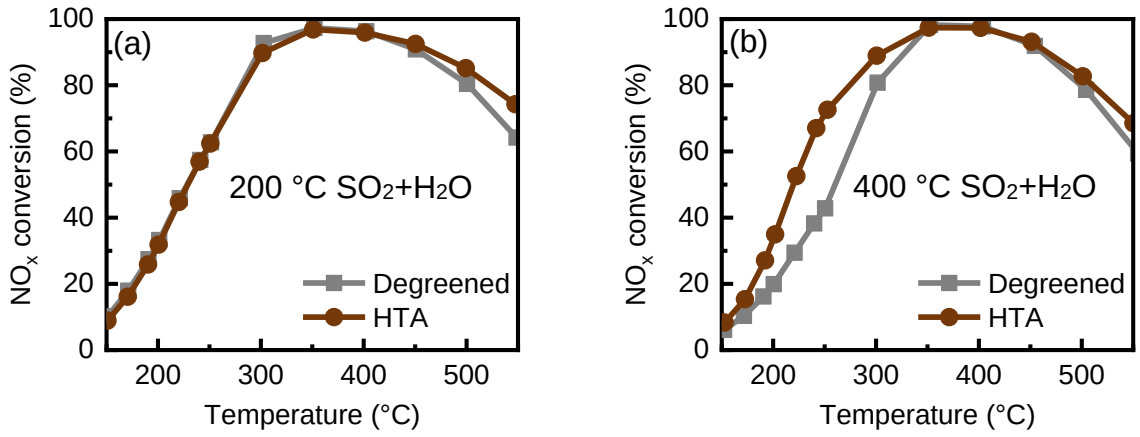


Fig. 2.6. SCR results obtained using the degreened and HTA catalysts after 50 ppm $SO_2$ exposure in the presence of 7% water at (a) 200 °C and (b) 400 °C for 6.5 h. The SCR reaction conditions are described in Table 2.1.

However, when comparing the extents of deactivation after the samples were exposed to $SO_2$ under dry or wet conditions at 200 °C, it is apparent that including water with $SO_2$ led to a loss in $NO_x$ conversion, as shown in Fig. 2.7 (a) and (b). In addition, when exposing the samples to $SO_2$ at 400 °C under wet or dry conditions, see Fig. 2.7 (c) and (d), the degreened catalyst led to a similar extent of deactivation whether water was included or not, but the $NO_x$ conversion over the HTA catalyst was still more impacted with water present. These results show that there is not only a dependency on $SO_2$ oxidation activity, but that there is also an additional effect of water. And this water + $SO_2$ effect is more significant, or becomes apparent, for the catalyst that showed weaker $SO_2$ oxidation activity under dry conditions. At 200 °C, the $SO_2$ oxidation activity is relatively poor over both catalysts, but during $SO_2$ exposure in the presence of water at 200 °C, for both the degreened and HTA catalysts, there is deactivation. Thus, this inclusion of water during the $SO_2$ exposure is relatively significant, and deactivation mainly stems from its effect over just $SO_2$ exposure alone. However, at 400 °C, the $SO_2$ oxidation activity of the degreened catalyst is relatively high, so the individual dependence on $SO_2$ oxidation activity is still observed. The $SO_2$ oxidation activity of the HTA catalyst is relatively lower, so the inclusion of water during the $SO_2$ exposure is more apparent than that for the degreened sample.

At this stage, we may only speculate as to the origin of this water effect. For example, one possible explanation is that the presence of water affects the catalytic oxidation of the S species. Water solvates copper sites leading to higher mobility [32,74], which might influence oxidation activity. We indeed found that $SO_2$ oxidation conversion to $SO_3$ is higher in the presence of water compared to in the absence of water, see in Appendix A, Fig. A8. This does not verify increased oxidation of surface sulfur species at lower temperatures, but does show improved oxidation at least. At 400 °C, the catalyst would be relatively dehydrated and an effect of water less likely.

However, there was still an effect of $H_2O$ during the 400 °C exposure, suggesting that even some residual $H_2O$ has an impact on oxidation. With $SO_3$ or oxidized surface sulfur species formation, $H_2SO_4$ formation is another possibility. For example, if $SO_2$ oxidation is strongly inhibited by product $SO_3$, as NO oxidation is by $NO_2$ [82], then it is possible the immediate formation of $H_2SO_4$ from $SO_3$ and $H_2O$ would diminish the $SO_3$ inhibition. Yet another possibility is the role of $H_2O$ itself as an oxidant, as has been proposed for $CH_4$ conversion to $CH_3OH$ over Cu-zeolite catalysts [83,84], which might influence the extent of $SO_2$ or surface sulfur species oxidation.

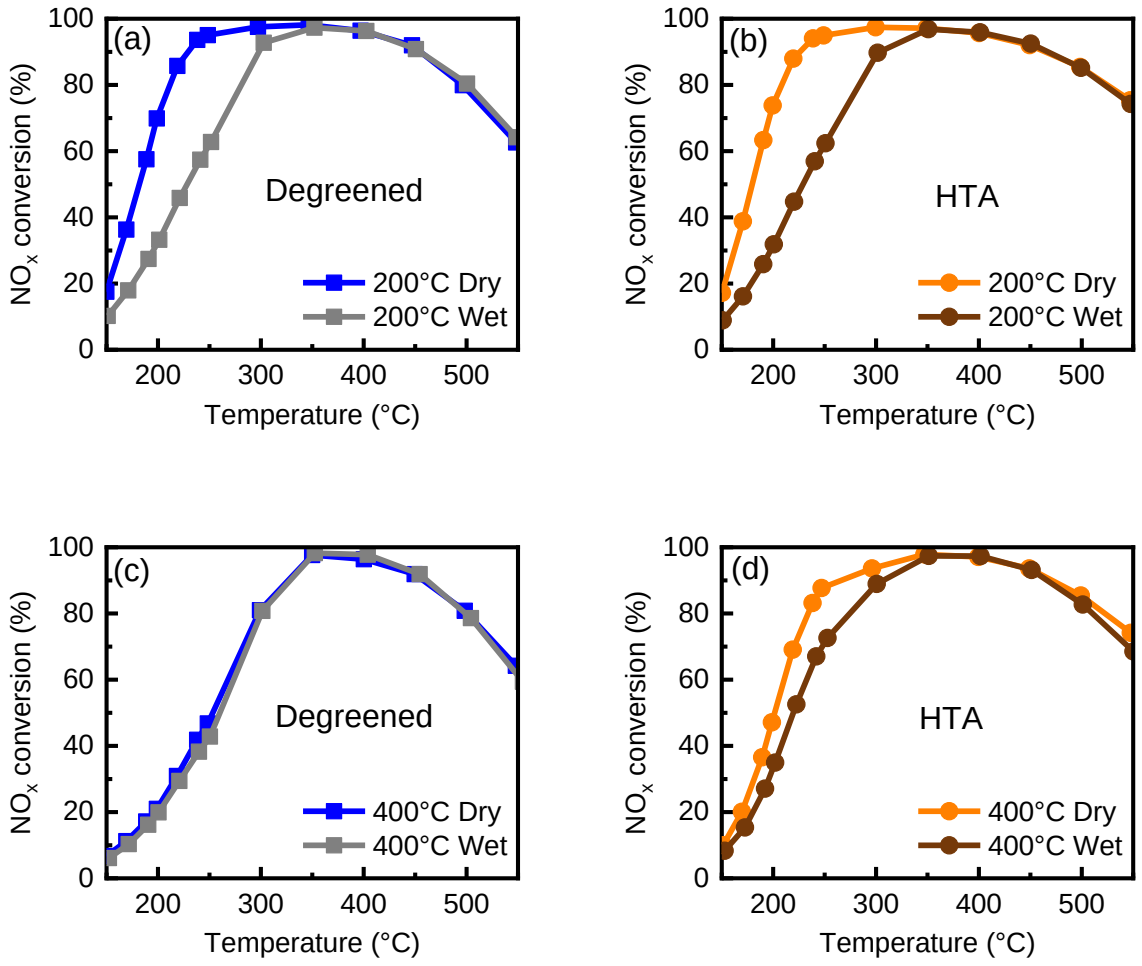


Fig. 2.7. SCR results comparing exposure to 50 ppm $SO_2$ in the presence and absence of 7% $H_2O$ for 6.5 h on the (a) degreened catalyst at 200 °C, (b) HTA catalyst at 200 °C, (c) degreened catalyst

at 400 °C, and (d) HTA catalyst at 400 °C. The SCR reaction conditions are described in Table 2.1.

The effect of water was further tested by comparing the effect of an intermediate water concentration during $SO_2$ exposure on the HTA catalyst, with results shown in Fig. 2.8. With 0.5% $H_2O$ during $SO_2$ exposure at 200 °C, there was an impact on the extent of $NO_x$ conversion loss, much like that when including 7% water. However, for the $SO_2$ exposure at 400°C, the addition of 0.5% water did not impact catalyst deactivation. Extrapolating on the idea of the water affecting $SO_2$ oxidation extent, the HTA catalyst has relatively poor oxidation activity at 200 °C under dry conditions, but with the addition of water either $SO_2$ or surface sulfur species oxidation is enhanced. The HTA catalyst has higher oxidation activity at 400 °C than at 200 °C, and is also more dehydrated especially with the smaller gas-phase $H_2O$ level, and therefore the effect of the smaller amount of water is again not as significant.

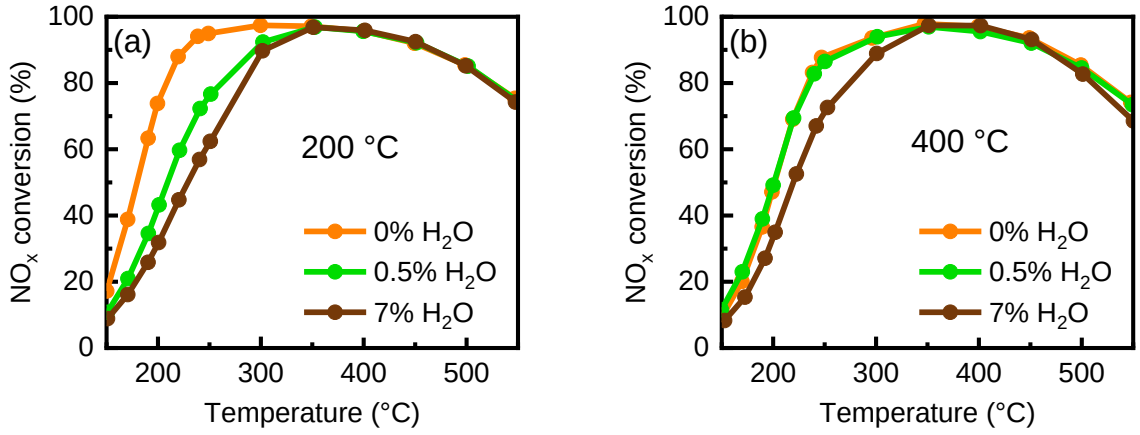


Fig. 2.8. SCR results after exposing the HTA catalyst to 50 ppm $SO_2$ for 6.5 h with different water concentrations: 0, 0.5, and 7% at (a) 200 °C and (b) 400 °C. The SCR reaction conditions are described in Table 2.1.

## 2.5 Conclusions

SCR of $NO_x$ by $NH_3$ over a Cu-SSZ-13 can be inhibited by sulfur poisoning. In terms of the commonly identified Cu species in this formulation, literature and our own data suggest that a sample with more Z2Cu relative to ZCuOH is less susceptible to sulfur poisoning under some conditions. Furthermore, the catalyst with more ZCuOH appears to be, in general, a better oxidation catalyst. Mild hydrothermal aging induces the migration of the Cu from ZCuOH to Z2Cu and at the same time leads to decreased CO, NO, $NH_3$ and $SO_2$ oxidation conversions. DRIFTS also correlates the change in $NH_3$ oxidation to a change in relative ZCuOH amounts. We here show a relationship between the extent of sulfur poisoning in the absence of water to the catalyst's oxidation ability. The results after different sulfur treatments, such as $SO_3$ exposure, higher temperature and higher $O_2$ concentration during $SO_2$ exposure all support a mechanism that includes surface $SO_2$ oxidation leading to more deactivation. This therefore implies that the extent of poisoning is dependent on the oxidation activity of the different Cu species, not solely on their relative amounts. For the case of sulfur exposure in the presence of water, similar trends were observed, with the extent of sulfur poisoning correlated to the catalyst's $SO_2$ oxidation reaction activity. However, the inclusion of water causes further deactivation during $SO_2$ exposure at 200 °C, and also at 400 °C, but to a lesser extent, likely due to a more dehydrated condition. We speculate that the inclusion of water affects oxidation reaction extents over this Cu-SSZ-13 catalyst.

## 2.6 Acknowledgements

The authors gratefully acknowledge Cummins Inc. for financial support. The authors also acknowledge Professor Chris Paolucci and Professor Robert Davis and their research groups for informative discussions.

# Chapter 3. Probing Cu Dimers before and after Sulfur Poisoning

## 3.1 Introduction

Cu-SSZ-13 is commonly used in the diesel engine after-treatment system as a catalyst to reduce $NO_x$. It can reach high $NO_x$ conversion over a wide range of temperatures, has good hydrothermal stability, and good hydrocarbon poisoning resistance compared to other Cu zeolite catalysts [16,24,51,61,63,85].

Even though Cu-SSZ-13 has advantages over other SCR catalysts and is commercially used, sulfur, an element in the diesel fuel and lubricant oil, can deactivate the catalyst. Two types of deactivation mechanisms have been proposed. One is pore-blocking by $SO_2$-related species [45,86–89]. The other proposed is that $SO_2$-related species poison the Cu active sites. Z2Cu and ZCuOH have been identified under inert conditions, and are the ion exchanged Cu associated with the active sites [25,32,39]. Prior studies showed that sulfur interacts with Z2Cu and ZCuOH differently. $SO_2$ is more likely to interact with ZCuOH and forms $CuSO_4$ species which requires relatively high temperature to decompose [44,49,50]. Based on this, Wei et al. and Xi et al. both found that catalysts after mild hydrothermal aging, which transforms ZCuOH to Z2Cu, were less poisoned by sulfur [58,73]. Our previous work in Chapter 2 further showed that the extent of sulfur poisoning had a strong correlation with the catalyst oxidation activity, which is influenced by the relative ZCuOH and Z2Cu amounts. With S species oxidation on the catalyst surface, more deactivation is observed [90].

A recent study showed that $SO_2$ reacts with $[Cu^{II}_2(NH_3)_4O_2]^{2+}$ dimers under SCR conditions [91]. Based on this study, we tried to understand whether other Cu dimers formation without $NH_3$ in the environment, such as ZCuOCuZ species, could react with sulfur species. Li et al. showed that the Cu-SSZ-13 sample with predominantly ZCuOH when synthesized could form Cu dimers

after high temperature treatment with $O_2$ [70]. Göltl et al. suggested that Z2Cu in a six member ring is too narrow for a dimer to form [92], which further supports that Cu dimers can only be formed by ZCuOH.

In this work, we further conducted SCR rate experiments to understand the sulfur poisoning and regeneration effects on the catalysts. We found that SCR reaction rate decreased after sulfur exposure. We hypothesize this decrease is likely due to the Cu dimers poisoned by sulfur species. CO titration and diffuse reflectance ultraviolet-visible (DR UV-Vis) spectroscopy were used to study the amount of the Cu dimers before and after sulfur poisoning. Da Costa et al. showed that $Cu^{2+}$ monomers cannot reduce with CO, but CO can react with Cu dimers and form $CO_2$ [93]. The reaction is shown in equation (3-1). By using this method, we can quantify and compare the $CO_2$ formed during CO exposure before and after sulfur exposure and using the stoichiometry in equation (3-1) can quantify the amount of Cu dimers on the catalyst.

$$[ZCu\text{-}O\text{-}CuZ]^{2+} + CO \rightarrow 2ZCu^{+} + CO_2 \quad (3\text{-}1)$$

In terms of DR UV-Vis spectroscopy, literature shows that four peaks representing ZCuOH and Cu dimers appear in the d-d transition region after catalysts containing ZCuOH are exposed to $O_2$ at high temperature [40,70,94]. We therefore used this technique to see if exposure to sulfur would affect this region and how.

### 3.2 Experimental Methods

A Cu-SSZ-13 monolith-supported catalyst with 600 cells per square inch (cpsi) cell density was provided by Cummins Inc. The catalysts were core drilled from the monolith, to 45 cells with 2.9 cm length for the experiments. Each piece of monolith catalyst was wrapped with ceramic fiber strings and loaded in a quartz tube, purchased from Quartz Scientific. The tube was then put in a

Lindberg Blue M furnace. Catalyst upstream and downstream temperatures were measured by K type thermocouples, purchased from Omega.

The total flow rate for each reactor experiment was 1403 sccm, which corresponds to a 60,000 $h^{-1}$ space velocity. Gas cylinders were purchased from Praxair. Gas flow rates were metered by mass flow controllers, purchased from MKS Instruments. The steam flow rate was metered by a controlled evaporation mixer (CEM) purchased from Bronkhorst. The carrier gas of the steam was $N_2$. Sulfinert tubing, purchased from Swagelok, was used to prevent corrosion by sulfur and limit its adsorption on the tubing walls. The tubing was heated to 150 °C. Gas mixture concentrations and catalyst outlet gas concentrations were monitored by a MKS MultiGas 2030 FT-IR.

Before experiments, a mild hydrothermal aging (HTA) was conducted at 650 °C for 5 h with the conditions listed in Table 3.1. For experiments with catalysts was not exposed to sulfur, an $O_2$ pretreatment was conducted at 500 °C for 1 h with the conditions listed in Table 3.1. Then the temperature was cooled to 150 °C for experiments. CO exposure and $NH_3$-SCR experimental conditions are listed in Table 3.2. CO titration experiments were done for 24 h if the catalyst was not exposed to sulfur. If the catalyst was exposed to sulfur, CO titration experiments were done long enough to make sure that the $CO_2$ concentration decreased to zero. SCR experiments were conducted in a steady-state condition and stepwise decreased temperature. $SO_2$ and $SO_2$ + $SO_3$ exposure were conducted at 425 °C. The total sulfur exposure corresponds to a loading on the catalyst of 55 g/L, i.e. this would be the loading if all sulfur adsorbed. If there was a regeneration process after sulfur exposure, it was conducted at 575 °C for 1 h with the conditions listed in Table 3.1. After sulfur exposure, an $O_2$ pretreatment was conducted at 400 °C, with a temperature ramp rate of 2 °C/min. The conditions are listed in Table 3.1. Based on the literature and our

experimental data, no sulfur was released up to or at 400 °C [48,95]. Then, the temperature was cooled to 150 °C for CO and SCR experiments.

Table 3.1 Pretreatment conditions

| Reactions | $SO_2$ (ppm) | $SO_3$ (ppm) | $H_2O$ (%) | $O_2$ (%) | $N_2$ |
|---|---|---|---|---|---|
| HTA | - | - | 7 | 10 | Balance |
| $O_2$ pretreatment | - | - | - | 10 | Balance |
| $SO_2$ exposure | 30 | - | 7 | 10 | Balance |
| $SO_2$ + $SO_3$ exposure | 5 | 25 | 7 | 10 | Balance |
| Regeneration after sulfur exposure* | - | - | 7 | 10 | Balance |

* If not specified, the regeneration process was not conducted.

Table 3.2 Reaction conditions used

| Reactions | $NH_3$ (ppm) | NO (ppm) | CO (ppm) | $H_2O$ (%) | $O_2$ (%) | $N_2$ |
|---|---|---|---|---|---|---|
| SCR | 200 | 200 | - | 7 | 10 | Balance |
| CO titration* | 200 | - | 1000 | - | - | Balance |

* Unless specified, CO titration was conducted at 150 °C.

Calculations include:

$$NO_x \text{ conversion during SCR reaction} = \frac{NO_{x_{in}} - NO_{x_{out}}}{NO_{x_{in}}} \times 100\% \quad (3\text{-}2)$$

A PerkinElmer Lambda 850 DR UV-vis spectrometer was used to characterize whether Cu dimers appear on the Cu-SSZ-13 catalyst before and after sulfur exposure. We used a Harrick Scientific Praying Mantis cell and UV grade $SiO_2$ windows. Catalyst powder was scraped from the monolith-supported catalysts before and after S exposure. These were filled into a sample cup

and the sample surface was leveled to the cup height. The total flow rate for these experiments was 50 sccm. The gas was Ultra Zero Air, purchased from Praxair, with 19.5 – 23.5% $O_2$, < 2 ppm $H_2O$, 0.5 ppm $CO_2$, 0.5 ppm CO, 0.5 ppm total hydrocarbon content, and balance $N_2$. Spectra were scanned before, during, and after a dry air pretreatment on the sample at 400 °C with dry air for 1 h.

### 3.3 Results and discussion

*Sulfur poisoning study without regeneration after sulfur exposure*

$NO_x$ conversions were measured at levels under 20%, using this as simply a rule of thumb type of value to obtain the SCR kinetic results, before and after sulfur exposure. The plot of conversions as a function of temperature is shown in Fig. 3.1 (a) and the SCR reaction pre-exponential and activation energy results are listed in Table 3.3. Dhillon et al. calculated the Weisz-Prater number of the SCR reaction on a Cu-SSZ-13 monolith catalyst with 66,000 $h^{-1}$ space velocity. They found that the number is larger than 1 when the reaction temperature is higher than 250 °C. Since their reaction conditions are similar to us, we assume that our results presented here were not in internal mass transfer limitation [96].

After $SO_2$ or $SO_2$ + $SO_3$ exposure without regeneration, catalyst $NO_x$ conversions decrease compared to the $NO_x$ conversion before sulfur exposure. The Arrhenius plots from the SCR results are shown in Fig. 3.1 (b). Both pre-exponential factor and activation energy values on the sulfur poisoned samples decreased from 93 kJ/mol (before sulfur poisoned) to 53 ($SO_2$ poisoned) and 55 ($SO_2$ + $SO_3$ poisoned) kJ/mol. The inclusion of $SO_3$ decreases the $NO_x$ conversion slightly more than that compared to $SO_2$ poisoning, but the SCR activation energy and pre-exponential factor after $SO_3$ poisoning are similar to those after $SO_2$ poisoning.

The values of the SCR reaction activation energy before and after sulfur exposure are also close to the values reported in the literature [44,58]. The decrease might be related to a mass transfer limitation or a change in the reaction mechanism, or rate determining step of the mechanism [97]. However, our current results cannot definitively differentiate which leads to the decrease of the activation energy.

If the activation change after sulfur exposure is not due to a mass transfer limitation, something in the SCR mechanism changes. The usually used SCR mechanism at low temperature, without sulfur exposure, is driven by two $Cu^{I}(NH_3)_2$ reacting with an $O_2$ molecule to form a $Cu(NH_3)_2$-$O_2$-$Cu(NH_3)_2$ dimer [33]. However, this Cu dimer species can react with sulfur species [91] and with its loss might lead to a decrease in SCR activity. Another possibility is that the $Cu(NH_3)_2$-$O_2$-$Cu(NH_3)_2$ dimer might not be able to form after sulfur exposure, with the Cu bound to sulfur inhibiting its mobility or ability to form the dimer. If so, the SCR reaction is not limited to the monomer.

The research of sulfur could react with Cu dimers led us to probe whether Cu dimers were still on the catalysts after sulfur exposure. We studied the static Cu dimers which are ZCu-O-CuZ like species, different from the literature that there was $NH_3$ on the catalyst [91]. To titrate the amount of static Cu dimers, literature shows that CO titration can be used, with the equation shown in equation (3-1) [93].

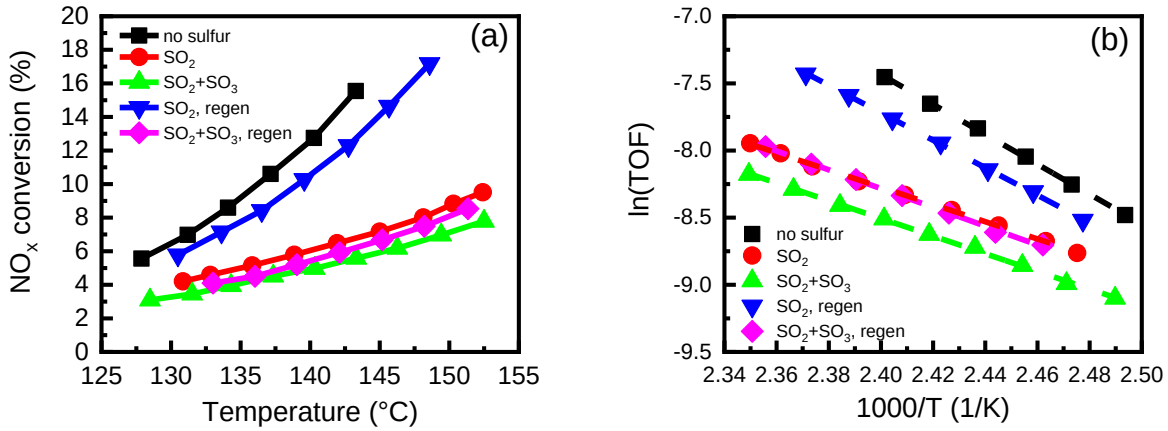


Fig. 3.1. (a) $NO_x$ conversions and (b) Arrhenius plots obtained during the SCR reaction with conditions described in Table 3.2. Catalysts include before sulfur exposure and with and without regeneration after $SO_2$ and $SO_2$ + $SO_3$ exposure.

Table 3.3 SCR reaction activation energies and pre-exponential factors measured using catalysts with different sulfur exposure conditions

| Conditions | No sulfur | $SO_2$ | $SO_2$ + $SO_3$ | $SO_2$, regen | $SO_2$ + $SO_3$, regen |
|---|---|---|---|---|---|
| Ea (kJ/mol) | 93 | 53 | 55 | 85 | 58 |
| A ($s^{-1}$) | $2.4 \times 10^8$ | $1.2 \times 10^3$ | $1.4 \times 10^3$ | $2.1 \times 10^7$ | $4.9 \times 10^3$ |

The results of CO titration experiments are listed in Table 3.4. After sulfur exposure without regeneration afterwards, the amount of $CO_2$ formed from CO titration experiments decreased significantly, from 29 μmol/g before S exposure to lower than 0.5 μmol/g. Based on the stoichiometry from Equation (3-1), the amount of Cu dimers can be obtained. The results show that Cu dimers cannot be titrated by CO after sulfur exposure, or were not formed. It implies that

Cu dimers are one of the sites that sulfur species can poison either by blocking their formation or blocking their ability to be titrated from CO.

Table 3.4 CO titration results after different sulfur exposure conditions

| Conditions | No sulfur | $SO_2$ | $SO_2 + SO_3$ | $SO_2$, regen | $SO_2 + SO_3$, regen |
|---|---|---|---|---|---|
| $CO_2$ (μmol/g) | 29 | 0.46 | 0.33 | 12.5 | 1.1 |

DR UV-Vis spectroscopy can be used to characterize some Cu species. Li et al. showed that after a high temperature $O_2$ pretreatment, 4 peaks were observed in the d-d transition region on catalysts with ZCuOH. These 4 peaks shrank to one single peak after CO exposure, leaving behind isolated ZCuOH [70]. If indeed these peaks characterize Cu dimer species, then if the CO titration results above accurately show that Cu dimers are not present after S exposure, then the UV-Vis peaks should also be absent.

The UV-Vis spectra for the catalyst before sulfur exposure are shown in Fig. 3.2. Three curves are shown in the spectra, which are spectra collected before, during, and after a 400 °C dry air pretreatment. Before a high temperature dry air pretreatment, there was only a peak shown in the d-d transition region. Moisture inhibits the Cu dimer formation. Giordanino et al. showed similar spectra with only one peak in the d-d transition region for hydrated Cu-SSZ-13 [40]. As there was no pretreatment for our sample, it is likely hydrated via ambient exposure. We also did a CO titration experiment with 7% $H_2O$ at 200 °C, see Fig. 3.2 (b). Little, 0.42 μmol/g, $CO_2$ was detected during the CO titration experiment. These results provide support that little to no Cu dimers were formed in a hydrated environment. During and after a high temperature dry air pretreatment, three

peaks are shown in the d-d transition region. The high temperature dry air pretreatment removed water in the catalyst, so that Cu dimers were formed. Since the UV-Vis spectrometer cannot scan the region higher than 900 nm, or lower than 11111 $cm^{-1}$, the fourth peak that is reported close to 10000 $cm^{-1}$ cannot be detected. The remaining three peak positions are similar to the peak positions reported in the literature [40,70].

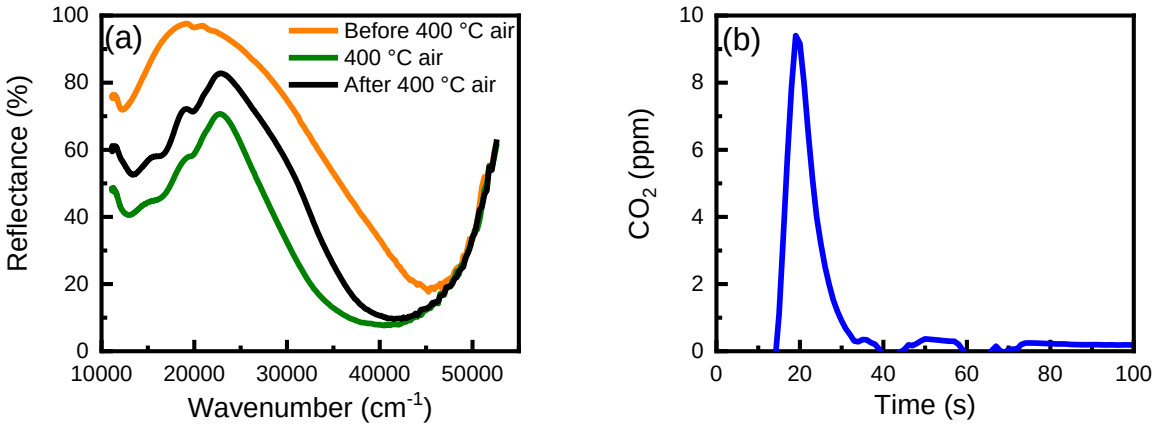


Fig. 3.2. DR UV-Vis spectra of the fresh catalyst before, during, and after a 400 °C dry air pretreatment. The spectra before and after the 400 °C dry air pretreatment were collected at 27 °C. (b) CO titration with 7% $H_2O$ included on the hydrothermally aged Cu-SSZ-13 catalyst. The gas concentration was 200 ppm CO, 7% $H_2O$ and balance $N_2$. This CO titration experiment was done at 200 °C.

The DR UV-Vis comparison spectra of all 5 catalysts with and without sulfur exposure are shown in Fig. 3.3. The spectra were collected after a 400 °C dry air pretreatment. The spectra obtained from catalysts that were exposed to sulfur without a following regeneration did not show a clear peak in the d-d transition region, see Fig. 3.3 (a). This suggests that both $SO_2$ and $SO_2$ +

$SO_3$ exposed catalysts lose most of the Cu dimers during sulfur exposure. The results are consistent with the CO titration results.

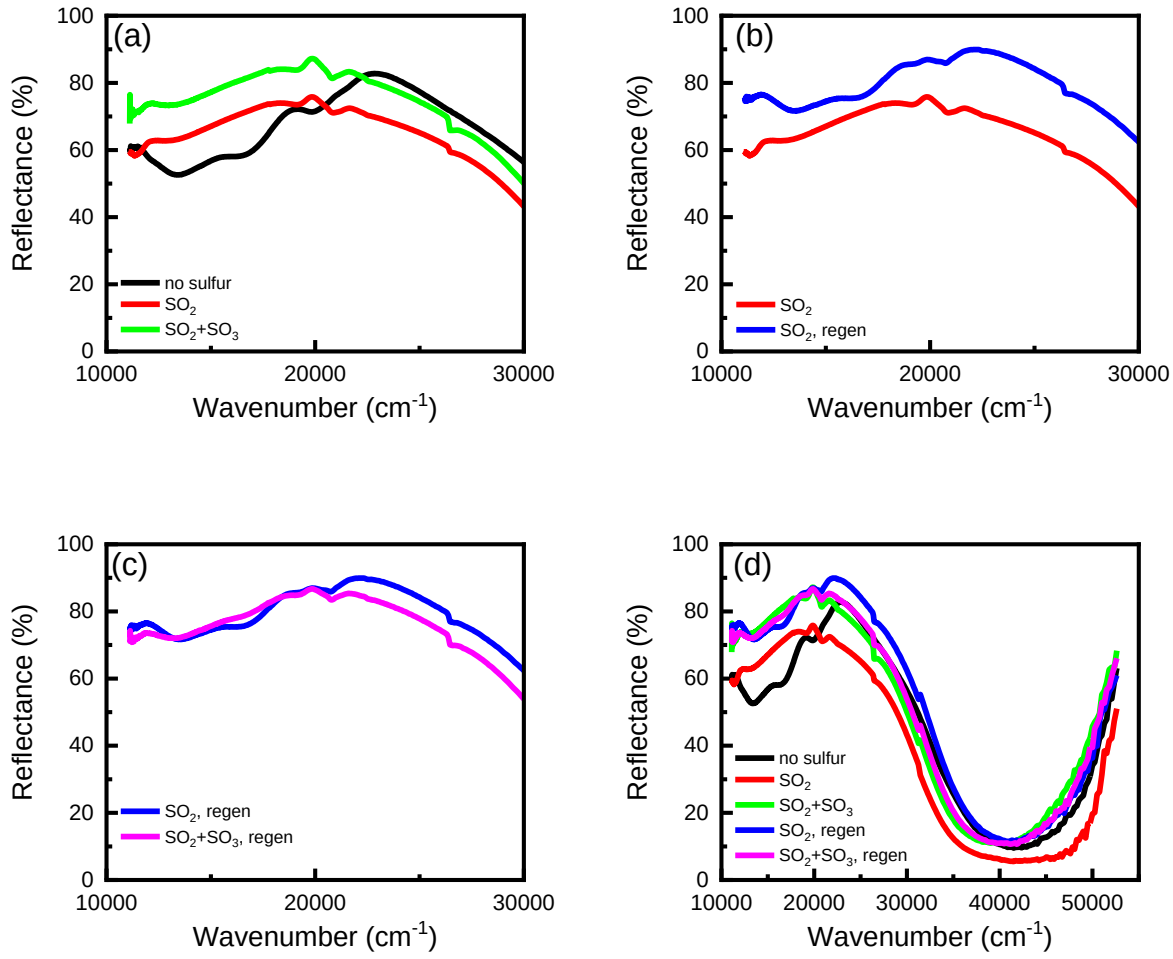


Fig. 3.3. DR UV-Vis spectra obtained from the Cu/SSZ-13 catalysts before and after $SO_2$ and $SO_2$ + $SO_3$ exposure, with and without regeneration. (a) Comparison spectra of catalysts before and after $SO_2$ and $SO_2$ + $SO_3$ exposure without regeneration. (b) Comparison spectra with and without regeneration after $SO_2$ exposure. (c) Comparison spectra with and without regeneration after $SO_2$ + $SO_3$ exposure. (d) Comparison of all 5 spectra. All 5 spectra were collected at 27 °C after a 400 °C dry air pretreatment for 1 h.

*Sulfur poisoning study with regeneration after sulfur exposure*

After regeneration at 575 °C, the $SO_2$ + $SO_3$ exposed catalyst has a slight improvement in $NO_x$ conversion compared to no regeneration, see Fig. 3.1 (a). The activation energy remained about the same, measured as 55 kJ/mol before and 58 kJ/mol after, see Table 3.3. The pre-exponential factor increased slightly, from $1.4 \times 10^3$ to $4.9 \times 10^3$, after regeneration compared to no regeneration. This suggests that some active sites were regenerated. This suggests overall that the high temperature regeneration used with the $SO_2$ + $SO_3$ exposed sample did not change the rate limiting step of the SCR reaction mechanism or mass transfer limitations were still maintained, compared to the case of no regeneration.

In the case of regeneration after $SO_2$ exposure, SCR $NO_x$ conversion increased and is close to the conversions obtained from the fresh catalyst. The activation energy and pre-exponential factor also increased and are similar to the original values. The increase in activation energy suggests that the SCR mechanism changes back to the original pathway, or the mass transfer limitations by sulfur are removed.

CO titration results show similar trends as the SCR rate results. Little $CO_2$ was formed, 1.1 μmol/g, when CO titrated the sample that was regenerated after $SO_2$ + $SO_3$ exposure, but 12.5 μmol/g of $CO_2$ was detected when CO titrated the sample that was regenerated after $SO_2$ exposure. The results suggest that the regeneration process recovered little Cu dimers for the sample that was poisoned by $SO_2$ + $SO_3$, but the regeneration process recovered a significant amount of Cu dimers for the sample that was poisoned by $SO_2$.

DR UV-Vis results, see Fig. 3.4, are also consistent with the CO titration results. The spectrum from the catalyst exposed to $SO_2$ and regeneration afterwards shows 3 peaks in the d-d transition

region, see Fig. 3.4 (b). This is consistent with the CO titration data that showed regeneration of $SO_2$ exposed catalyst can recover Cu dimers. On the other hand, the spectrum of the catalyst exposed to $SO_2$ + $SO_3$ and regeneration afterwards does not contain such distinct peaks in the d-d transition region, see Fig. 3.4 (c). This is again consistent with the CO titration data where regeneration of the $SO_2$ + $SO_3$ exposed catalyst can only recover a limited amount of the originally observed Cu dimers.

It is interesting to note that the regeneration process did not have a clear impact on the sample that was poisoned by $SO_2$ + $SO_3$, but it did on the sample that was poisoned by $SO_2$. A possible explanation is that there were at least two sulfur species formed during sulfur exposure. Assuming so, one of them is more stable than the other. The more stable species formed either from $SO_3$ in the feed binding with Cu sites or from $SO_2$ oxidation on the Cu sites to a more oxidized S species. The less stable species was formed by $SO_2$ binding on the Cu sites, possibly forming $CuHSO_3$ species [44]. Deka et al. did a TPD experiment on a 0.41 wt% of sulfur loaded field aged Cu-SSZ-13 catalyst. They assigned a $SO_2$ release peak at 590 °C to copper bisulfite, formed as in reaction, and assigned another $SO_2$ release peak at 680 °C to copper bisulfate [95]. These assignments might explain our results. The 575 °C regeneration can lead to the decomposition of the copper bisulfite but cannot decompose the copper bisulfate. However, those TPD results are not further supported by other characterization techniques, so such assignments need more verification. For example, Su et al. did TPD experiments with a sulfur poisoned Cu-SSZ-13 catalyst and they assigned the peak at around 600 °C to copper sulfate [48]. Thus, we can only hypothesize that there are two different sulfur species. The exact species require further characterization.

## 3.4 Conclusions

In this portion of the research, we studied how exposure of a Cu-SSZ-13 catalyst to $SO_2$ or $SO_2 + SO_3$ impacted the SCR conversion as well as number of Cu dimer sites that could be titrated by CO exposure. From the SCR experiments, the SCR reaction activation energy and pre-exponential factor decreased after $SO_2$ or $SO_2 + SO_3$ poisoning. CO titration and UV-Vis results both show that catalysts lost Cu dimers after sulfur poisoning.

In terms of regeneration impact, the regeneration process led to more significantly recovered conversion for the catalyst exposed to $SO_2$ compared to the catalyst exposed to $SO_2 + SO_3$. The SCR reaction pre-exponential factor and activation energy of the catalyst exposed to $SO_2$ both increased after regeneration. The CO titration and UV-Vis results suggest that Cu dimers were recovered during regeneration. On the other hand, regeneration of the catalyst exposed to $SO_2 + SO_3$ only led to a slight increase in the pre-exponential factor, and the activation energy did not change. The CO titration and UV-Vis results again followed the SCR reaction test trend, with little recovery of UV-Vis features associated with dimers and no $CO_2$ formed during the CO titration experiment. The different impact of regeneration on $SO_2$ exposed and $SO_2 + SO_3$ exposed catalysts are hypothesized to be because of two different sulfur species formed on the catalyst.

## 3.5 Acknowledgements

The authors gratefully acknowledge Cummins Inc. for financial support. The authors also acknowledge Professor Chris Paolucci, Keka Mandal, and Asanka Wijerathne whose research using DFT calculations initially showed that sulfur species bind on Cu dimers strongly. Finally, the authors acknowledge both Professor Chris Paolucci and Professor Robert Davis and their research groups for informative discussions.

# Chapter 4. Ethylene Effect on Cu Sites Transformation during Hydrothermal Aging

## 4.1 Introduction

The inhomogeneous fuel and air mixture in the diesel engine leads to different types of emissions, such as unburned hydrocarbons, CO, $NO_x$, $SO_x$, and particular matter. A typical diesel engine aftertreatment system contains a diesel oxidation catalyst (DOC), diesel particular filter (DPF), and selective catalytic reduction (SCR) and ammonia slip catalysts (ASC). Even though the DOC upstream of the SCR catalyst oxidizes most of the hydrocarbons and CO, there are still some ppm levels of hydrocarbons detected before the SCR catalyst [98,99], particularly during the cold-start period [26,100–102], where the temperature of the DOC is not high enough to oxidize the hydrocarbons.

Hydrocarbon poisoning of SCR catalysts has been researched. Cu-ZSM-5, Cu-beta, Fe-ZSM-5, and Fe-beta were first investigated, and the SCR reaction conversions over all four catalysts decreased with exposure to propylene ($C_3H_6$) [85,98,100,101,103]. Luo et al. investigated $C_3H_6$ poisoning and dodecane poisoning over Cu-beta and Cu-CHA catalysts. They found that the small-pore catalyst, Cu-CHA, could resist both $C_3H_6$ and dodecane poisoning compared to the Cu-beta catalyst [85]. Even though the Cu-CHA catalyst can better resist the hydrocarbon poisoning, Ma et al. reported that the Cu-SSZ-13 catalyst still suffered from $C_3H_6$ poisoning during SCR reactions [104].

Hydrothermal aging at high temperatures is another factor resulting in deactivation of SCR catalysts. Even though the hydrothermal stability of the Cu-CHA catalyst is higher compared to other Cu-zeolite catalysts, Cu-CHA still suffers from hydrothermal aging deactivation if the temperatures are too high [52–55]. Some literature further investigated the extent of hydrocarbon

poisoning before and after the hydrothermal aging [19,102]. The extent of hydrocarbon poisoning on Cu-SSZ-13 became more severe after hydrothermal aging compared to the extent of hydrocarbon poisoning on the fresh catalyst [19,102].

One area that has not been explored is the effect of hydrocarbons in the composition of the gas stream during hydrothermal aging. In this study, we used $C_2H_4$ as a representative short chain hydrocarbon, see Fig. 4.1, and show that after 1 hour of mild hydrothermal aging at 600 °C, 100% conversion of $C_2H_4$ was no longer observed and that the conversion slowly decreased with further time. We found that high temperature SCR and oxidation activity of the Cu-SSZ-13 catalyst after HTA with $C_2H_4$ included was affected when compared to HTA with no $C_2H_4$ included. We hypothesized that either the formation of coke hinders the Cu sites transformation from ZCuOH to Z2Cu or a back transformation from Z2Cu to ZCuOH occurs during HTA + $C_2H_4$. Other effects of hydrothermal aging with other different exhaust components included on SCR performance were also investigated.

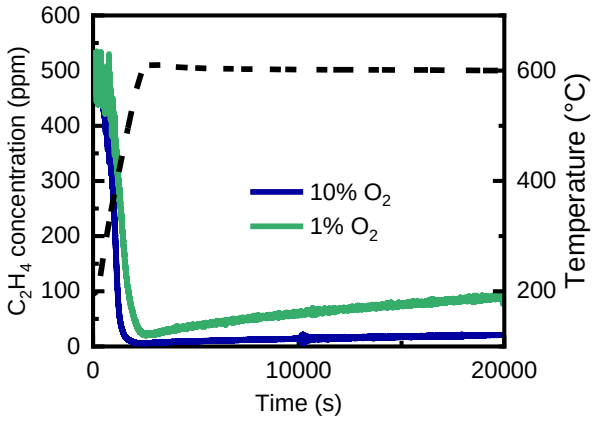


Fig. 4.1. Comparison of $C_2H_4$ concentration change during HTA + $C_2H_4$. The aging condition is detailed in Table 4.1 in the Experimental Methods section. In one experiment 1% $O_2$ was included in the other 10% $O_2$.

## 4.2 Experimental Methods

The catalysts used in the experiments were taken from a Cu-SSZ-13 washcoated monolith provided by Cummins Inc. The cell density of the monolith is 300 cpsi and 21 cells with 2.9 cm in length of the monolith were used in the experiments. Every catalyst was wrapped with ceramic fiber strings before loading into a quartz tube, purchased from Quartz Scientific. The tube was then placed in a Lindberg Blue M furnace. The upstream and downstream temperatures of the catalyst were measured by K-type thermocouples purchased from Omega.

The total flow rate for all reactor experiments was 1360 sccm, which corresponds to a 62,300 $h^{-1}$ space velocity. NO, $NH_3$, CO, $C_2H_4$, $N_2$, $O_2$, and $CO_2$ gases were used in the experiments. Gas cylinders were either purchased from Praxair or Matheson. A $N_2$ generator, purchased from Parker Balston, was used for the supplementary $N_2$. Gas flow rates were metered by mass flow controllers (MFC), purchased from MKS Instrument. The steam flow rate was metered by a controlled evaporator mixer (CEM), purchased from Bronkhorst. The carrier gas for the steam was $N_2$. All reactor tubing was kept at 150 °C using heating tapes and wrapped insulation.

A mild hydrothermal aging at 600 °C for 25 h with different simulated exhaust mixtures was conducted before experiments. Details of the concentrations are listed in Table 4.1. Prior to each experiment, an $O_2$ pretreatment with 10% $O_2$ and $N_2$ balance at 500 °C was conducted for 1 h. After the $O_2$ pretreatment, the temperature was cooled to 150 or 200 °C depending on the experiment. Gas concentration details for each experiment are listed in Table 4.2. $NH_3$-SCR, $NH_3$ oxidation, and NO oxidation experiments were conducted under steady-state conditions, starting from 200 °C (150 °C if the experiment is SCR) and stepwise increasing to 550 °C, while CO

oxidation was conducted with a temperature program, starting from 200 °C and with a 10 °C/min of increasing rate to 550 °C.

Table 4.1 Mild hydrothermal aging at 600 °C for 25 h with different exhaust conditions

| Conditions | $O_2$ (%) | $H_2O$ (%) | $CO_2$ (%) | $NH_3$ (ppm) | NO (ppm) | CO (ppm) | $C_2H_4$ (ppm) | $N_2$ |
|---|---|---|---|---|---|---|---|---|
| HTA | 10 | 7 | 8 | - | - | - | - | Balance |
| HTA + $NH_3$ | 10 | 7 | 8 | 200 | - | - | - | Balance |
| HTA + NO | 10 | 7 | 8 | - | 200 | - | - | Balance |
| HTA + CO | 10 | 7 | 8 | - | - | 200 | - | Balance |
| HTA + $C_2H_4$ | 10* | 7 | 8 | - | - | - | 500 | Balance |

* If not specified, 10% $O_2$ was used during HTA + $C_2H_4$.

Table 4.2 Reaction conditions used

| Reactions | $NH_3$ (ppm) | NO (ppm) | CO (ppm) | $SO_2$ (ppm) | $H_2O$ (%) | $CO_2$ (%) | $O_2$ (%) | $N_2$ |
|---|---|---|---|---|---|---|---|---|
| SCR | 200 | 200 | - | - | 7 | 8 | 10 | Balance |
| NO oxidation | - | 200 | - | - | 7 | 8 | 10 | Balance |
| $NH_3$ oxidation | 200 | - | - | - | 7 | 8 | 10 | Balance |

| | | | | | | | | |
|---|---|---|---|---|---|---|---|---|
| CO oxidation | - | - | 200 | - | 7 | - | 10 | Balance |

Calculations include:

$NO_x$ conversion during SCR reaction = $\frac{NO_{x_{in}} - NO_{x_{out}}}{NO_{x_{in}}} \times 100\%$ (4-1)

NO oxidation conversion = $\frac{NO_{in} - NO_{out}}{NO_{in}} \times 100\%$ (4-2)

$NH_3$ oxidation conversion = $\frac{NH_{3_{in}} - NH_{3_{out}}}{NH_{3_{in}}} \times 100\%$ (4-3)

CO oxidation conversion = $\frac{CO_{in} - CO_{out}}{CO_{in}} \times 100\%$ (4-4)

$NH_3$ adsorption experiments with diffuse reflectance infrared Fourier transform spectroscopy (DRIFTS) was used to characterize the T-O-T vibration region of catalysts after the HTA with exposure to different simulated exhaust mixtures. A Nicolet iS-50 FT-IR spectrometer with a Harrick Scientific Praying Mantis cell and ZnSe windows were used. Catalyst powder was scraped from the monolith-supported catalysts. The powder was filled into a sample cup and the sample surface was leveled to the cup height. A mixture of dry ice and isopropanol was used as a cold trap to remove residual water from the inlet line into the cell. The total flow rate for all experiments and treatments was 50 sccm. Before experiments, catalysts were exposed to 10% $O_2$ and balance He at 500 °C for 1 h ($O_2$ pretreatment). Then, the system was cooled to 120 °C. The background spectrum was taken after the catalyst had cooled to the target temperature. For $NH_3$ adsorption experiments, the experiments were conducted at 120 °C with 1000 ppm $NH_3$ and balance He.

## 4.3 Results and Discussion

*Catalyst oxidation activity decreases less after HTA + $C_2H_4$ compared to after just HTA*

SCR reaction conversion results before and after mild HTA are shown in Fig. 4.2 (a). Below 350 °C, similar $NO_x$ conversions are obtained. The results are consistent with the literature [49,52,62,63,74] and the results shown in Chapter 2. Above 350 °C, the HTA catalyst resulted in a higher $NO_x$ conversion compared to the fresh catalyst. SCR reactions at high temperatures are affected by the $NH_3$ oxidation reaction, which becomes significant at high temperatures, shown in Fig. 4.2 (b). The loss of $NH_3$ reacting with $O_2$ instead of NO leads to the loss of $NO_x$ conversion at high temperatures [17,49,63].

The SCR performance after HTA with different exhaust components included were measured to understand the effect of these components on the catalyst aging. The results are shown in Fig. 4.2 (c). In this set of experiments, $NH_3$, NO, and CO were chosen as different components. The results show that these have little impact on the catalyst changes during HTA. However, SCR performance at high temperatures increased slightly less after HTA + $C_2H_4$, compared to HTA. The results are shown in Fig. 4.2 (a). From previous discussion, SCR performance at high temperatures is affected by $NH_3$ oxidation reactions. The results in Fig. 4.2 (b) illustrate that the $NH_3$ oxidation activity of the catalyst after HTA + $C_2H_4$ was higher than that after HTA, which is consistent with the previous discussion.

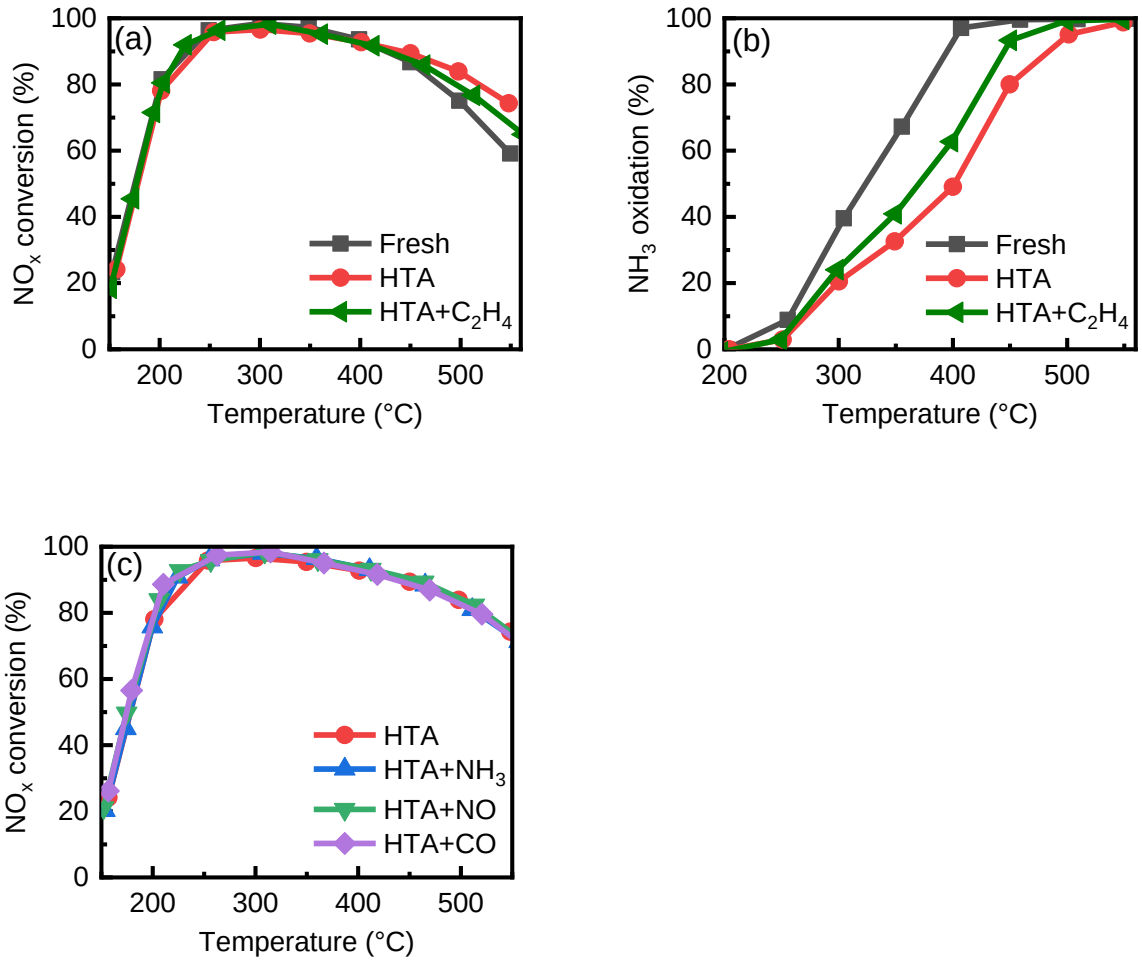


Fig. 4.2. Comparison of (a) SCR performance and (b) $NH_3$ oxidation performance before and after HTA and HTA + $C_2H_4$ and (c) the SCR performance after HTA + $NH_3$ or NO or CO. The aging conditions are listed in Table 4.1 and the SCR reaction conditions are listed in Table 4.2. Note that fresh catalyst was not hydrothermally aged.

DRIFTS characterization was used to help understand the change in $NH_3$ oxidation and SCR performance after HTA + $C_2H_4$ compared to after HTA only. Based on the literature, the T-O-T vibration region of the DRIFTS spectra, 850 – 1000 $cm^{-1}$, can be used to distinguish the relative amount of ZCuOH and Z2Cu by $NH_3$ adsorption [39,44,56,63], results shown in Fig. 4.3. The 900 $cm^{-1}$ peak is assigned to $NH_3$ adsorption on Z2Cu and the 950 $cm^{-1}$ peak is assigned to $NH_3$

adsorption on ZCuOH [39,44,56,63]. The 900 $cm^{-1}$ peak was normalized for better comparison of the 950 $cm^{-1}$ peak between fresh (before HTA), HTA, and HTA + $C_2H_4$. The results show that HTA + $C_2H_4$ had a "lower" peak than HTA. This indicates that the proportion of ZCuOH/Z2Cu is more on the HTA + $C_2H_4$ sample compared to that of the HTA sample. Literature [17,49,76] has shown that the catalyst $NH_3$ oxidation activity is related to the amount of ZCuOH. The DRIFTS results and the literature explain that the difference of the $NH_3$ oxidation activity between the catalyst after HTA and HTA + $C_2H_4$ is due to a different amount of ZCuOH.

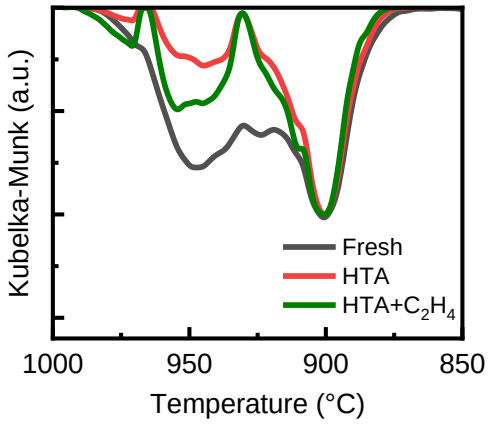


Fig. 4.3. DRIFTS spectra of $NH_3$ adsorption on fresh (before HTA), HTA, and HTA + $C_2H_4$ samples. The aging conditions are listed in Table 4.1. $NH_3$ adsorption conditions: 1000 ppm $NH_3$ and balance He at 120 °C.

There are two possible hypotheses to explain why the amount of ZCuOH on the catalysts changed after including $C_2H_4$ during the mild hydrothermal aging. The first one is pore blocking caused by $C_2H_4$ which slightly hinders the ZCuOH transformation to Z2Cu during HTA. The second is a back transformation of Z2Cu to ZCuOH. Here, only the second hypothesis was tested. The results are shown in Fig. 4.4. A 50 h HTA was first done, to transform some ZCuOH to Z2Cu. Then, a 25 h HTA + $C_2H_4$ was done with the same catalyst that had experienced 50 h HTA. The

comparison of SCR performance shown in Fig. 4.4 (a) shows that the hydrothermal aging with ethylene after 50 h HTA had slightly lower $NO_x$ conversion above 400 °C. The higher temperature SCR performance difference between two aging conditions indicates that the ZCuOH amounts in the catalyst after these two different aging conditions are different. To be specific, the catalyst after the additional hydrothermal aging with ethylene has more than the catalyst that only experienced 50 h HTA. If ethylene does not have any effect during the hydrothermal aging process, less ZCuOH amount should be expected. Thus, the results imply that a back transformation from Z2Cu to ZCuOH occurred when including ethylene during mild hydrothermal aging. The $NH_3$ oxidation comparison results, shown in Fig. 4.4 (b), support this finding. The $NH_3$ oxidation activity of the catalyst after additional HTA + $C_2H_4$ is higher than that after HTA only. Based on the previous discussion that $NH_3$ oxidation activity is related to the amount of ZCuOH, the catalyst after additional HTA + $C_2H_4$ had more ZCuOH than the catalyst after HTA only. Furthermore, NO oxidation and CO oxidation performance, shown in Fig. 4.4 (c) and (d), were also done and they both show the same trend as $NH_3$ oxidation.

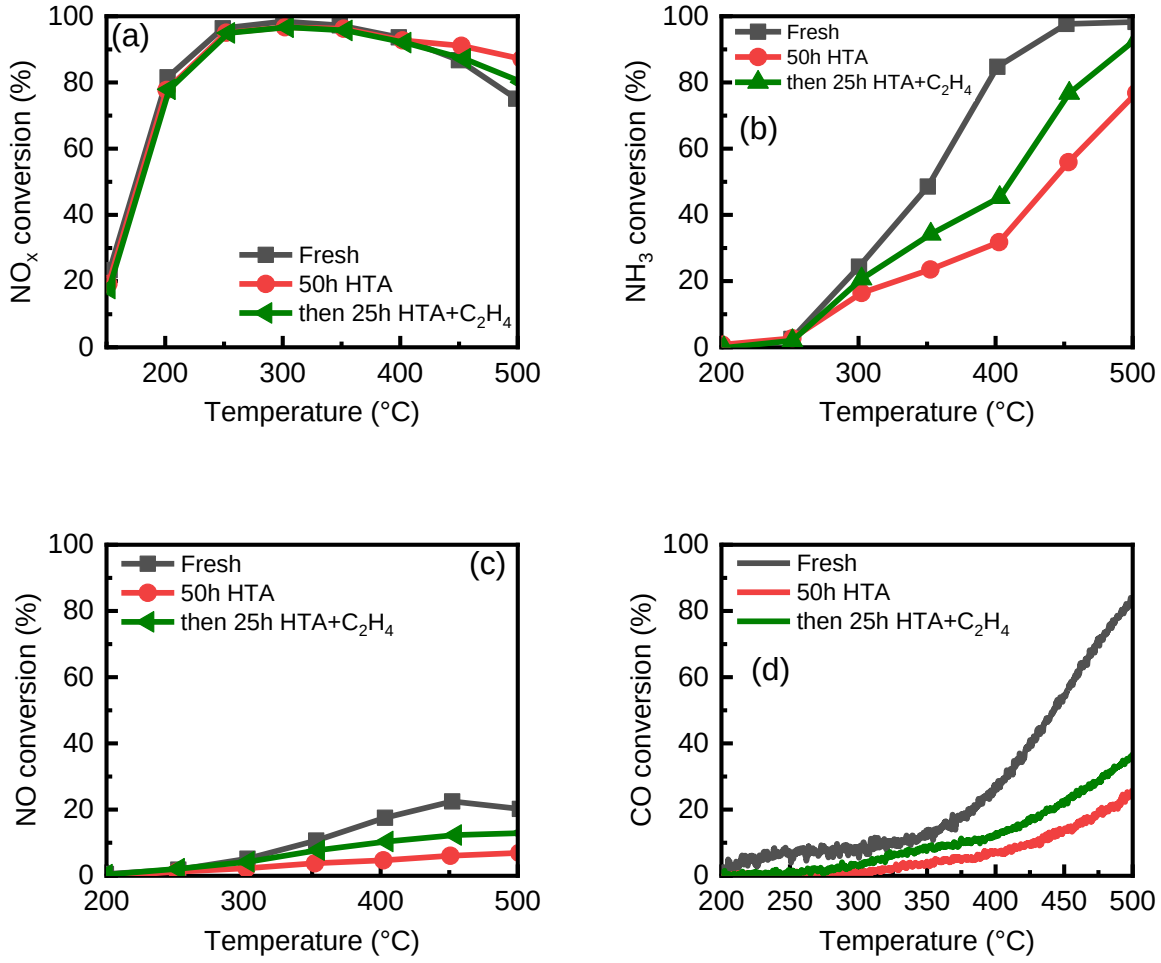


Fig. 4.4. (a) $NH_3$-SCR, (b) $NH_3$ oxidation, (c) NO oxidation, and (d) CO oxidation performance comparison between the catalyst before HTA, the catalyst after 50 h HTA and the catalyst after additional 25 h HTA + $C_2H_4$ after 50 h HTA. The SCR, $NH_3$ oxidation, NO, and CO oxidation conditions are listed in Table 4.2. The HTA conditions are listed in Table 4.1.

The DRIFTS experiments with $NH_3$ adsorption as a probe technique were used to further characterize the amount of ZCuOH and Z2Cu between catlaysts before HTA, after 50 h HTA, and the additional HTA + $C_2H_4$ after 50 h HTA. The results are shown in Fig. 4.5. The 900 $cm^{-1}$ peaks were normalized to compare the 950 $cm^{-1}$ peaks between samples. The results show that the peak intensity of the catalyst after additional HTA + $C_2H_4$ is slightly higher than the catalyst

after 50 h HTA only. The results again illustrate that the ZCuOH amount of the catalyst after additional HTA + $C_2H_4$ is more than the catalyst after 50 h HTA. This further supports that a back transformation from Z2Cu to ZCuOH occurred after including ethlyene during HTA.

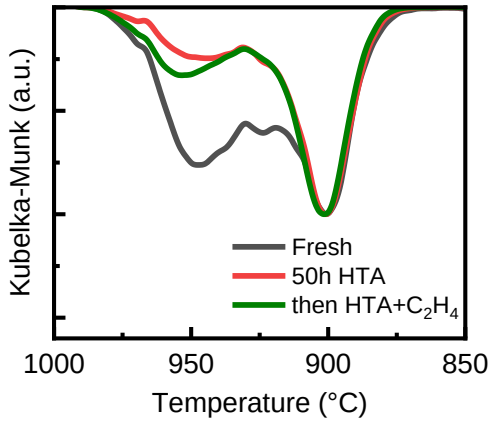


Fig. 4.5. DRIFTS spectra of $NH_3$ adsorption on fresh (before HTA), 50 h HTA, and an additional 25 h HTA + $C_2H_4$ after 50 h HTA samples. The aging conditions are listed in Table 4.1. $NH_3$ adsorption conditions: 1000 ppm $NH_3$ and balance He at 120 °C.

**4.4 Conclusions**

Catalyst SCR performance and oxidation conversion are measured after hydrothermal aging with different exhaust mixtures. We found that mild hydrothermal aging with ethylene leads to high-temperature SCR reaction conversion decrease and $NH_3$ oxdiation conversion increase compared to the same after mild hydrothermal aging without ethylene included. DRIFTS spectra showed that the Cu distribution changed between mild hydrothermal aging with and without ethylene. We propose that the inclusion of ethylene can transform part of the Z2Cu to ZCuOH. An additional mild hydrothermal aging with ethylene after 50 h of mild hydrothermal aging was conducted to test this. The SCR raciton conversion decreased and $NH_3$, NO, and CO oxidation conversion increased compared to the performance after 50 h mild hydrothermal aging. The

DRIFTS spectra show that the ZCuOH peak intensity after the additional mild hydrothermal aging with ethylene is greater than the ZCuOH peak intensity after 50 h mild hydrothermal aging. These DRIFTS and oxidaiton results support the hypothesis that the Z2Cu transforms to ZCuOH during HTA, opposite of the nornal trends.

### 4.5 Acknowledgements

The authors gratefully acknowledge Cummins Inc. for financial support. The authors also acknowledge Dr. Marina Cortés-Reyes for the initial reactor setup and the informative discussions.

## References


[1] P. Breeze, Diesel Engines, in: Pist. Engine-Based Power Plant, 2018: pp. 47–57. https://doi.org/10.1016/B978-0-12-812904-3.00005-7.

[2] H. Jääskeläinen, M.K. Khair, Diesel engines, (2021). https://doi.org/10.1201/b13974.

[3] Y.B. Zeldovich, 26. Oxidation of Nitrogen in Combustion and Explosions, in: Sel. Work. Yakov Borisovich Zeldovich, Vol. I, 1992: pp. 404–410. https://doi.org/10.1515/9781400862979.404.

[4] A. Kumar, M.A. Smith, K. Kamasamudram, N.W. Currier, A. Yezerets, Chemical de$SO_x$: An effective way to recover Cu-zeolite SCR catalysts from sulfur poisoning, Catal. Today. 267 (2016) 10–16. https://doi.org/10.1016/j.cattod.2016.01.033.

[5] DieselNet, Emission Test Cycles: HD FTP Transient, (2019). https://www.dieselnet.com/standards/cycles/ftp_trans.php.

[6] DieselNet, Emission Test Cycles FTP-75, (2019) 20–22. https://dieselnet.com/standards/cycles/ftp75.php%0Ahttps://www.dieselnet.com/standards/cycles/ftp75.php.

[7] R.K. Lattanzio, J.E. McCarthy, Tier 3 motor vehicle emission and fuel standards, U.S. EU Mot. Veh. Stand. Elem. Considerations Trade Issues. (2014) 37–54.

[8] M. Koebel, M. Elsener, M. Kleemann, Urea-SCR: a promising technique to reduce $NO_x$ emissions from automotive diesel engines, Catal. Today. 59 (2000) 335–345. https://doi.org/10.1016/S0920-5861(00)00299-6.

[9] M. Kleemann, M. Elsener, M. Koebel, A. Wokaun, Hydrolysis of isocyanic acid on SCR

catalysts, Ind. Eng. Chem. Res. 39 (2000) 4120–4126. https://doi.org/10.1021/ie9906161.

[10] S. Brandenberger, O. Kröcher, A. Tissler, R. Althoff, The state of the art in selective catalytic reduction of $NO_x$ by ammonia using metal-exchanged zeolite catalysts, Catal. Rev. - Sci. Eng. 50 (2008) 492–531. https://doi.org/10.1080/01614940802480122.

[11] A. Grossale, I. Nova, E. Tronconi, D. Chatterjee, M. Weibel, The chemistry of the $NO/NO_2$-$NH_3$ "fast" SCR reaction over Fe-ZSM5 investigated by transient reaction analysis, J. Catal. 256 (2008) 312–322. https://doi.org/10.1016/j.jcat.2008.03.027.

[12] F. Gao, E.D. Walter, E.M. Karp, J. Luo, R.G. Tonkyn, J.H. Kwak, J. Szanyi, C.H.F. Peden, Structure-activity relationships in $NH_3$-SCR over Cu-SSZ-13 as probed by reaction kinetics and EPR studies, J. Catal. 300 (2013) 20–29. https://doi.org/10.1016/j.jcat.2012.12.020.

[13] F. Gao, J.H. Kwak, J. Szanyi, C.H.F. Peden, Current Understanding of Cu-Exchanged Chabazite Molecular Sieves for Use as Commercial Diesel Engine $DeNO_x$ Catalysts, Top. Catal. 56 (2013) 1441–1459. https://doi.org/10.1007/s11244-013-0145-8.

[14] K. Kamasamudram, C. Henry, N. Currier, A. Yezerets, $N_2O$ Formation and Mitigation in Diesel Aftertreatment Systems, SAE Int. J. Engines. 5 (2012) 688–698. https://doi.org/10.4271/2012-01-1085.

[15] G. Cavataio, J. Girard, J.E. Patterson, C. Montreuil, Y. Cheng, C.K. Lambert, Laboratory testing of urea-SCR formulations to meet tier 2 bin 5 emissions, SAE Tech. Pap. 2007 (2007) 776–790. https://doi.org/10.4271/2007-01-1575.

[16] J.H. Kwak, D. Tran, S.D. Burton, J. Szanyi, J.H. Lee, C.H.F. Peden, Effects of hydrothermal aging on $NH_3$-SCR reaction over Cu/zeolites, J. Catal. 287 (2012) 203–209.

https://doi.org/10.1016/j.jcat.2011.12.025.

[17] J.M. González, A.L. Villa, High Temperature SCR Over Cu-SSZ-13 and Cu-SSZ-13 + Fe-SSZ-13: Activity of $Cu^{2+}$ and $[CuOH]^{1+}$ Sites and the Apparent Promoting Effect of Adding Fe into Cu-SSZ-13 Catalyst, Catal. Letters. 151 (2021) 3011–3019. https://doi.org/10.1007/s10562-021-03550-7.

[18] F. Gao, Fe-exchanged small-pore zeolites as ammonia selective catalytic reduction ($NH_3$-SCR) catalysts, Catalysts. 10 (2020) 1–33. https://doi.org/10.3390/catal10111324.

[19] A. Wang, Y. Wang, E.D. Walter, N.M. Washton, Y. Guo, G. Lu, C.H.F. Peden, F. Gao, $NH_3$-SCR on Cu, Fe and Cu + Fe exchanged beta and SSZ-13 catalysts: Hydrothermal aging and propylene poisoning effects, Catal. Today. 320 (2019) 91–99. https://doi.org/10.1016/j.cattod.2017.09.061.

[20] D. Zhang, R.T. Yang, $N_2O$ Formation Pathways over Zeolite-Supported Cu and Fe Catalysts in $NH_3$-SCR, Energy and Fuels. 32 (2018) 2170–2182. https://doi.org/10.1021/acs.energyfuels.7b03405.

[21] K. Kamasamudram, N. Currier, T. Szailer, A. Yezerets, Why Cu- and Fe-zeolite SCR catalysts behave differently at low temperatures, SAE Int. J. Fuels Lubr. 3 (2010) 664–672. https://doi.org/10.4271/2010-01-1182.

[22] S.A. Bates, A.A. Verma, C. Paolucci, A.A. Parekh, T. Anggara, A. Yezerets, W.F. Schneider, J.T. Miller, W.N. Delgass, F.H. Ribeiro, Identification of the active Cu site in standard selective catalytic reduction with ammonia on Cu-SSZ-13, J. Catal. 312 (2014) 87–97. https://doi.org/10.1016/j.jcat.2014.01.004.

[23] K. Leistner, O. Mihai, K. Wijayanti, A. Kumar, K. Kamasamudram, N.W. Currier, A. Yezerets, L. Olsson, Comparison of Cu/BEA, Cu/SSZ-13 and Cu/SAPO-34 for ammonia-SCR reactions, Catal. Today. 258 (2015) 49–55. https://doi.org/10.1016/j.cattod.2015.04.004.

[24] J.H. Kwak, R.G. Tonkyn, D.H. Kim, J. Szanyi, C.H.F. Peden, Excellent activity and selectivity of Cu-SSZ-13 in the selective catalytic reduction of $NO_x$ with $NH_3$, J. Catal. 275 (2010) 187–190. https://doi.org/10.1016/j.jcat.2010.07.031.

[25] F. Gao, D. Mei, Y. Wang, J. Szanyi, C.H.F. Peden, Selective Catalytic Reduction over Cu/SSZ-13: Linking Homo- and Heterogeneous Catalysis, J. Am. Chem. Soc. 139 (2017) 4935–4942. https://doi.org/10.1021/jacs.7b01128.

[26] Y. Zheng, M.P. Harold, D. Luss, Effects of CO, $H_2$ and $C_3H_6$ on Cu-SSZ-13 catalyzed $NH_3$-SCR, Catal. Today. 264 (2016) 44–54. https://doi.org/10.1016/j.cattod.2015.06.028.

[27] A.M. Beale, I. Lezcano-Gonzalez, W.A. Slawinksi, D.S. Wragg, Correlation between Cu ion migration behaviour and de$NO_x$ activity in Cu-SSZ-13 for the standard $NH_3$-SCR reaction, Chem. Commun. 52 (2016) 6170–6173. https://doi.org/10.1039/c6cc00513f.

[28] F. Giordanino, E. Borfecchia, K.A. Lomachenko, A. Lazzarini, G. Agostini, E. Gallo, A. V. Soldatov, P. Beato, S. Bordiga, C. Lamberti, Interaction of $NH_3$ with Cu-SSZ-13 catalyst: A complementary FTIR, XANES, and XES study, J. Phys. Chem. Lett. 5 (2014) 1552–1559. https://doi.org/10.1021/jz500241m.

[29] S.Y. Joshi, A. Kumar, J. Luo, K. Kamasamudram, N.W. Currier, A. Yezerets, New insights into the mechanism of $NH_3$-SCR over Cu- and Fe-zeolite catalyst: Apparent negative activation energy at high temperature and catalyst unit design consequences, Appl. Catal. B

Environ. 226 (2018) 565–574. https://doi.org/10.1016/j.apcatb.2017.12.076.

[30] F. Gramigni, N.D. Nasello, N. Usberti, U. Iacobone, T. Selleri, W. Hu, S. Liu, X. Gao, I. Nova, E. Tronconi, Transient Kinetic Analysis of Low-Temperature $NH_3$-SCR over Cu-CHA Catalysts Reveals a Quadratic Dependence of Cu Reduction Rates on $Cu^{II}$, ACS Catal. 11 (2021) 4821–4831. https://doi.org/10.1021/acscatal.0c05362.

[31] C. Paolucci, A.A. Verma, S.A. Bates, V.F. Kispersky, J.T. Miller, R. Gounder, W.N. Delgass, F.H. Ribeiro, W.F. Schneider, Isolation of the copper redox steps in the standard selective catalytic reduction on Cu-SSZ-13, Angew. Chemie - Int. Ed. 53 (2014) 11828–11833. https://doi.org/10.1002/anie.201407030.

[32] C. Paolucci, A.A. Parekh, I. Khurana, J.R. Di Iorio, H. Li, J.D.A. Caballero, A.J. Shih, T. Anggara, W.N. Delgass, T. Miller, F.H. Ribeiro, R. Gounder, W.F. Schneider, Catalysis in a Cage : Condition-Dependent Speciation and Dynamics of Exchanged Cu Cations in SSZ-13 Zeolites, J. Am. Chem. Soc. (2016). https://doi.org/10.1021/jacs.6b02651.

[33] C. Paolucci, I. Khurana, A.A. Parekh, S. Li, A.J. Shih, H. Li, J.R. Di Iorio, J.D. Albarracin-caballero, A. Yezerets, J.T. Miller, W.N. Delgass, F.H. Ribeiro, W.F. Schneider, R. Gounder, Dynamic multinuclear sites formed by mobilized copper ions in $NO_x$ selective catalytic reduction, Science 357 (2017) 898–903.

[34] W. Hu, U. Iacobone, F. Gramigni, Y. Zhang, X. Wang, S. Liu, C. Zheng, I. Nova, X. Gao, E. Tronconi, Unraveling the Hydrolysis of $Z2Cu^{2+}$ to $ZCu^{2+}(OH)^-$ and Its Consequences for the Low-Temperature Selective Catalytic Reduction of NO on Cu-CHA Catalysts, ACS Catal. (2021) 11616–11625. https://doi.org/10.1021/acscatal.1c02761.

[35] E. Borfecchia, P. Beato, S. Svelle, U. Olsbye, C. Lamberti, S. Bordiga, Cu-CHA-a model

system for applied selective redox catalysis, Chem. Soc. Rev. 47 (2018) 8097–8133. https://doi.org/10.1039/c8cs00373d.

[36] A. Kumar, M.A. Smith, K. Kamasamudram, N.W. Currier, H. An, A. Yezerets, Impact of different forms of feed sulfur on small-pore Cu-zeolite SCR catalyst, Catal. Today. 231 (2014) 75–82. https://doi.org/10.1016/j.cattod.2013.12.038.

[37] H.-Y. Chen, Urea-SCR Technology for de$NO_x$ After Treatment of Diesel Exhausts, 1st ed., Springer New York, NY, 2014. https://doi.org/10.1007/978-1-4899-8071-7_5.

[38] D.W. Fickel, R.F. Lobo, Copper coordination in Cu-SSZ-13 and Cu-SSZ-16 investigated by variable-temperature XRD, J. Phys. Chem. C. 114 (2010) 1633–1640. https://doi.org/10.1021/jp9105025.

[39] J. Hun Kwak, H. Zhu, J.H. Lee, C.H.F. Peden, J. Szanyi, Two different cationic positions in Cu-SSZ-13?, Chem. Commun. 48 (2012) 4758–4760. https://doi.org/10.1039/c2cc31184d.

[40] F. Giordanino, P.N.R. Vennestrøm, L.F. Lundegaard, F.N. Stappen, S. Mossin, P. Beato, S. Bordiga, C. Lamberti, Characterization of Cu-exchanged SSZ-13: A comparative FTIR, UV-Vis, and EPR study with Cu-ZSM-5 and Cu-β with similar Si/Al and Cu/Al ratios, Dalt. Trans. 42 (2013) 12741–12761. https://doi.org/10.1039/c3dt50732g.

[41] C.W. Andersen, M. Bremholm, P.N.R. Vennestrøm, A.B. Blichfeld, L.F. Lundegaard, B.B. Iversen, Location of $Cu^{2+}$ in CHA zeolite investigated by X-ray diffraction using the Rietveld/maximum entropy method, IUCrJ. 1 (2014) 382–386. https://doi.org/10.1107/S2052252514020181.

[42] Y. Cheng, C. Lambert, D. Heui, J. Hun, S. June, C.H.F. Peden, The different impacts of $SO_2$ and $SO_3$ on Cu/zeolite SCR catalysts, Catal. Today. 151 (2010) 266–270. https://doi.org/10.1016/j.cattod.2010.01.013.

[43] Y. Jangjou, M. Ali, Q. Chang, D. Wang, J. Li, A. Kumar, W.S. Epling, Effect of $SO_2$ on $NH_3$ oxidation over a Cu-SAPO-34 SCR catalyst, Catal. Sci. Technol. 6 (2016) 2679–2685. https://doi.org/10.1039/c5cy02212f.

[44] Y. Jangjou, Q. Do, Y. Gu, L.G. Lim, H. Sun, D. Wang, A. Kumar, J. Li, L.C. Grabow, W.S. Epling, Nature of Cu Active Centers in Cu-SSZ-13 and Their Responses to $SO_2$ Exposure, ACS Catal. 8 (2018) 1325–1337. https://doi.org/10.1021/acscatal.7b03095.

[45] K. Wijayanti, K. Leistner, S. Chand, A. Kumar, K. Kamasamudram, N.W. Currier, A. Yezerets, L. Olsson, Deactivation of Cu-SSZ-13 by $SO_2$ exposure under SCR conditions, Catal. Sci. Technol. 6 (2016) 2565–2579. https://doi.org/10.1039/c5cy01288k.

[46] L. Zhang, D. Wang, Y. Liu, K. Kamasamudram, J. Li, W. Epling, $SO_2$ poisoning impact on the $NH_3$-SCR reaction over a commercial Cu-SAPO-34 SCR catalyst, Appl. Catal. B Environ. 156–157 (2014) 371–377. https://doi.org/10.1016/j.apcatb.2014.03.030.

[47] Y. Jangjou, Q. Do, Y. Gu, L.G. Lim, H. Sun, D. Wang, A. Kumar, J. Li, L.C. Grabow, W.S. Epling, Nature of Cu Active Centers in Cu-SSZ-13 and Their Responses to $SO_2$ Exposure, ACS Catal. 8 (2018) 1325–1337. https://doi.org/10.1021/acscatal.7b03095.

[48] W. Su, Z. Li, Y. Zhang, C. Meng, J. Li, Identification of sulfate species and their influence on SCR performance of Cu/CHA catalyst, Catal. Sci. Technol. 7 (2017) 1523–1528. https://doi.org/10.1039/c7cy00302a.

[49] J. Luo, D. Wang, A. Kumar, J. Li, K. Kamasamudram, N. Currier, A. Yezerets, Identification of two types of Cu sites in Cu/SSZ-13 and their unique responses to hydrothermal aging and sulfur poisoning, Catal. Today. 267 (2016) 3–9. https://doi.org/10.1016/j.cattod.2015.12.002.

[50] A.J. Shih, I. Khurana, H. Li, J. González, A. Kumar, C. Paolucci, T.M. Lardinois, C.B. Jones, J.D. Albarracin Caballero, K. Kamasamudram, A. Yezerets, W.N. Delgass, J.T. Miller, A.L. Villa, W.F. Schneider, R. Gounder, F.H. Ribeiro, Spectroscopic and kinetic responses of Cu-SSZ-13 to $SO_2$ exposure and implications for $NO_x$ selective catalytic reduction, Appl. Catal. A Gen. 574 (2019) 122–131. https://doi.org/10.1016/j.apcata.2019.01.024.

[51] D.W. Fickel, E. D'Addio, J.A. Lauterbach, R.F. Lobo, The ammonia selective catalytic reduction activity of copper-exchanged small-pore zeolites, Appl. Catal. B Environ. 102 (2011) 441–448. https://doi.org/10.1016/j.apcatb.2010.12.022.

[52] S.J. Schmieg, S.H. Oh, C.H. Kim, D.B. Brown, J.H. Lee, C.H.F. Peden, D.H. Kim, Thermal durability of Cu-CHA $NH_3$-SCR catalysts for diesel $NO_x$ reduction, Catal. Today. 184 (2012) 252–261. https://doi.org/10.1016/j.cattod.2011.10.034.

[53] Y.J. Kim, J.K. Lee, K.M. Min, S.B. Hong, I.S. Nam, B.K. Cho, Hydrothermal stability of Cu-SSZ-13 for reducing $NO_x$ by $NH_3$, J. Catal. 311 (2014) 447–457. https://doi.org/10.1016/j.jcat.2013.12.012.

[54] J. Song, Y. Wang, E.D. Walter, N.M. Washton, D. Mei, L. Kovarik, M.H. Engelhard, S. Prodinger, Y. Wang, C.H.F. Peden, F. Gao, Toward Rational Design of Cu / SSZ-13 Selective Catalytic Reduction Catalysts : Implications from Atomic-Level Understanding

of Hydrothermal Stability, (2017). https://doi.org/10.1021/acscatal.7b03020.

[55] F. Gao, J. Szanyi, On the hydrothermal stability of Cu/SSZ-13 SCR catalysts, Appl. Catal. A Gen. 560 (2018) 185–194. https://doi.org/10.1016/j.apcata.2018.04.040.

[56] J. Luo, F. Gao, K. Kamasamudram, N. Currier, C.H.F. Peden, A. Yezerets, New insights into Cu/SSZ-13 SCR catalyst acidity. Part I: Nature of acidic sites probed by $NH_3$ titration, J. Catal. 348 (2017) 291–299. https://doi.org/10.1016/j.jcat.2017.02.025.

[57] A. Kumar, M.A. Smith, K. Kamasamudram, N.W. Currier, H. An, A. Yezerets, Impact of different forms of feed sulfur on small-pore Cu-zeolite SCR catalyst, Catal. Today. 231 (2014) 75–82. https://doi.org/10.1016/j.cattod.2013.12.038.

[58] Y. Xi, C. Su, N.A. Ottinger, Z.G. Liu, Effects of hydrothermal aging on the sulfur poisoning of a Cu-SSZ-13 SCR catalyst, Appl. Catal. B Environ. 284 (2021) 119749. https://doi.org/10.1016/j.apcatb.2020.119749.

[59] Q. Ye, L. Wang, R.T. Yang, Activity, propene poisoning resistance and hydrothermal stability of copper exchanged chabazite-like zeolite catalysts for SCR of NO with ammonia in comparison to Cu/ZSM-5, Appl. Catal. A Gen. 427–428 (2012) 24–34. https://doi.org/10.1016/j.apcata.2012.03.026.

[60] P.G. Blakeman, E.M. Burkholder, H.Y. Chen, J.E. Collier, J.M. Fedeyko, H. Jobson, R.R. Rajaram, The role of pore size on the thermal stability of zeolite supported Cu SCR catalysts, Catal. Today. 231 (2014) 56–63. https://doi.org/10.1016/j.cattod.2013.10.047.

[61] L. Ma, Y. Cheng, G. Cavataio, R.W. McCabe, L. Fu, J. Li, Characterization of commercial Cu-SSZ-13 and Cu-SAPO-34 catalysts with hydrothermal treatment for $NH_3$-SCR of $NO_x$

in diesel exhaust, Chem. Eng. J. 225 (2013) 323–330. https://doi.org/10.1016/j.cej.2013.03.078.

[62] J. Luo, H. An, K. Kamasamudram, N. Currier, A. Yezerets, T. Watkins, L. Allard, Impact of Accelerated Hydrothermal Aging on Structure and Performance of Cu-SSZ-13 SCR Catalysts, SAE Int. J. Engines. 8 (2015) 1181–1186. https://doi.org/10.4271/2015-01-1022.

[63] D. Wang, Y. Jangjou, Y. Liu, M.K. Sharma, J. Luo, J. Li, K. Kamasamudram, W.S. Epling, A comparison of hydrothermal aging effects on $NH_3$-SCR of $NO_x$ over Cu-SSZ-13 and Cu-SAPO-34 catalysts, Appl. Catal. B Environ. 165 (2015) 438–445. https://doi.org/10.1016/j.apcatb.2014.10.020.

[64] I. Bull, W. Xue, P. Burk, R.S. Boorse, W.M. Jaglowski, G.S. Koermer, A. Moini, J.A. Patchett, J.C. Dettling, M.T. Claude, United State Patent No: US 7,601,662 B2, 2 (2009). https://patents.google.com/patent/US7601662B2/en.

[65] P.J. Andersen, H. Chen, M. Fedeyko, G. Mills, E. Weigert, (12) United States Patent, 2 (2012).

[66] Y. Jangjou, D. Wang, A. Kumar, J. Li, W.S. Epling, $SO_2$ Poisoning of the $NH_3$-SCR Reaction over Cu-SAPO-34: Effect of Ammonium Sulfate versus Other S-Containing Species, ACS Catal. 6 (2016) 6612–6622. https://doi.org/10.1021/acscatal.6b01656.

[67] A. Wang, L. Olsson, Insight into the $SO_2$ poisoning mechanism for $NO_x$ removal by $NH_3$-SCR over Cu/LTA and Cu/SSZ-13, Chem. Eng. J. 395 (2020) 125048. https://doi.org/10.1016/j.cej.2020.125048.

[68] M. Shen, Y. Zhang, J. Wang, C. Wang, J. Wang, Nature of $SO_3$ poisoning on Cu/SAPO-34

SCR catalysts, J. Catal. 358 (2018) 277–286. https://doi.org/10.1016/j.jcat.2017.12.008.

[69] R. Villamaina, F. Gramigni, U. Iacobone, S. Liu, I. Nova, E. Tronconi, M.P. Ruggeri, J. Collier, A.P.E. York, D. Thompsett, The $H_2O$ effect on Cu speciation in Cu-CHA-catalysts for $NH_3$-SCR probed by $NH_3$ titration, Catalysts. 11 (2021) 1–11. https://doi.org/10.3390/catal11070759.

[70] H. Li, C. Paolucci, I. Khurana, L.N. Wilcox, F. Göltl, J.D. Albarracin-Caballero, A.J. Shih, F.H. Ribeiro, R. Gounder, W.F. Schneider, Consequences of exchange-site heterogeneity and dynamics on the UV-visible spectrum of Cu-exchanged SSZ-13, Chem. Sci. 10 (2019) 2373–2384. https://doi.org/10.1039/c8sc05056b.

[71] H. Lee, I. Song, S.W. Jeon, D.H. Kim, Inter-particle migration of Cu ions in physically mixed Cu-SSZ-13 and H-SSZ-13 treated by hydrothermal aging, React. Chem. Eng. 4 (2019) 1059–1066. https://doi.org/10.1039/C8RE00281A.

[72] J. Luo, K. Kamasamudram, N. Currier, A. Yezerets, $NH_3$-TPD methodology for quantifying hydrothermal aging of Cu/SSZ-13 SCR catalysts, Chem. Eng. Sci. 190 (2018) 60–67. https://doi.org/10.1016/j.ces.2018.06.015.

[73] L. Wei, D. Yao, F. Wu, B. Liu, X. Hu, X. Li, X. Wang, Impact of Hydrothermal Aging on $SO_2$ Poisoning over Cu-SSZ-13 Diesel Exhaust SCR Catalysts, Ind. Eng. Chem. Res. 58 (2019) 3949–3958. https://doi.org/10.1021/acs.iecr.8b04543.

[74] H. Lee, I. Song, S.W. Jeon, D.H. Kim, Mobility of Cu Ions in Cu-SSZ-13 Determines the Reactivity of Selective Catalytic Reduction of $NO_x$ with $NH_3$, Phys. Chem. Lett. (2021) 1–7. https://doi.org/10.1021/acs.jpclett.1c00181.

[75] Y. Xi, N.A. Ottinger, C.J. Keturakis, Z.G. Liu, Dynamics of low temperature $N_2O$ formation under SCR reaction conditions over a Cu-SSZ-13 catalyst, Appl. Catal. B Environ. 294 (2021). https://doi.org/10.1016/j.apcatb.2021.120245.

[76] A.M. Beale, F. Gao, I. Lezcano-Gonzalez, C.H.F. Peden, J. Szanyi, Recent advances in automotive catalysis for $NO_x$ emission control by small-pore microporous materials, Chem. Soc. Rev. 44 (2015) 7371–7405. https://doi.org/10.1039/c5cs00108k.

[77] F. Gao, N.M. Washton, Y. Wang, M. Kollár, J. Szanyi, C.H.F. Peden, Effects of Si/Al ratio on Cu/SSZ-13 $NH_3$-SCR catalysts: Implications for the active Cu species and the roles of Brønsted acidity, J. Catal. 331 (2015) 25–38. https://doi.org/10.1016/j.jcat.2015.08.004.

[78] Y. Ma, X. Wu, S. Cheng, L. Cao, L. Liu, Y. Xu, J. Liu, R. Ran, Z. Si, D. Weng, Relationships between copper speciation and Brønsted acidity evolution over Cu-SSZ-13 during hydrothermal aging, Appl. Catal. A Gen. 602 (2020) 117650. https://doi.org/10.1016/j.apcata.2020.117650.

[79] L. Ma, Y. Cheng, G. Cavataio, R.W. McCabe, L. Fu, J. Li, In situ DRIFTS and temperature-programmed technology study on $NH_3$-SCR of $NO_x$ over Cu-SSZ-13 and Cu-SAPO-34 catalysts, Appl. Catal. B Environ. 156–157 (2014) 428–437. https://doi.org/10.1016/j.apcatb.2014.03.048.

[80] D. Wang, L. Zhang, K. Kamasamudram, W. Epling, In situ-DRIFTS Study of Selective Catalytic Reduction of $NO_x$ by $NH_3$ over Cu-Exchanged SAPO-34, ACS Catal. 3 (2013) 871–881. https://doi.org/10.1021/cs300843k | ACS Catal. 2013, 3, 871−881.

[81] X. Auvray, M. Arvanitidou, Å. Högström, J. Jansson, S. Fouladvand, L. Olsson, Comparative Study of $SO_2$ and $SO_2/SO_3$ Poisoning and Regeneration of Cu/BEA and

Cu/SSZ-13 for $NH_3$ SCR, Emiss. Control Sci. Technol. 7 (2021) 232–246. https://doi.org/10.1007/s40825-021-00203-4.

[82] T. Selleri, F. Gramigni, I. Nova, E. Tronconi, NO oxidation on Fe- and Cu-zeolites mixed with $BaO/Al_2O_3$ : Free oxidation regime and relevance for the $NH_3$-SCR chemistry at low temperature, Appl. Catal. B Environ. 225 (2018) 324–331. https://doi.org/10.1016/j.apcatb.2017.11.068.

[83] H. Zhang, J. Lv, Z. Zhang, C. Du, S. Wang, J. Lin, S. Wan, Y. Wang, H. Xiong, Oxidation of Methane to Methanol by Water Over Cu/SSZ-13: Impact of Cu Loading and Formation of Active Sites, ChemCatChem. 14 (2022). https://doi.org/10.1002/cctc.202101609.

[84] V.L. Sushkevich, D. Palagin, M. Ranocchiari, J.A. Van Bokhoven, Selective anaerobic oxidation of methane eables direct synthesis of methanol, Science 356 (2017) 523–527.

[85] J.Y. Luo, A. Yezerets, C. Henry, H. Hess, K. Kamasamudram, H.Y. Chen, W.S. Epling, Hydrocarbon poisoning of Cu-zeolite SCR catalysts, SAE Tech. Pap. (2012). https://doi.org/10.4271/2012-01-1096.

[86] L. Zhang, D. Wang, Y. Liu, K. Kamasamudram, J. Li, W. Epling, $SO_2$ poisoning impact on the $NH_3$-SCR reaction over a commercial Cu-SAPO-34 SCR catalyst, Appl. Catal. B Environ. 156–157 (2014) 371–377. https://doi.org/10.1016/j.apcatb.2014.03.030.

[87] C. Wang, Z. Chen, J. Wang, J. Wang, M. Shen, Unraveling the nature of sulfur poisoning on Cu/SSZ-13 as a selective reduction catalyst, J. Taiwan Inst. Chem. Eng. 118 (2021) 38–47. https://doi.org/10.1016/j.jtice.2020.12.033.

[88] D.W. Brookshear, J.G. Nam, K. Nguyen, T.J. Toops, A. Binder, Impact of sulfation and

desulfation on $NO_x$ reduction using Cu-chabazite SCR catalysts, Catal. Today. 258 (2015) 359–366. https://doi.org/10.1016/j.cattod.2015.04.029.

[89] H. Jiang, B. Guan, X. Peng, Y. Wei, R. Zhan, H. Lin, Z. Huang, Effect of sulfur poisoning on the performance and active sites of Cu/SSZ-13 catalyst, Chem. Eng. Sci. 226 (2020) 115855. https://doi.org/10.1016/j.ces.2020.115855.

[90] Y.-R. Chen, L. Wei, A. Kumar, D. Wang, W.S. Epling, How changes in Cu-SSZ-13 catalytic oxidation activity via mild hydrothermal aging influence sulfur poisoning extents, Catal. Sci. Technol. 12 (2022) 6891–6902. https://doi.org/10.1039/d2cy01394k.

[91] A.Y. Molokova, E. Borfecchia, A. Martini, I.A. Pankin, C. Atzori, O. Mathon, S. Bordiga, F. Wen, P.N.R. Vennestrøm, G. Berlier, T.V.W. Janssens, K.A. Lomachenko, $SO_2$ Poisoning of Cu-CHA de$NO_x$ Catalyst: The Most Vulnerable Cu Species Identified by X-ray Absorption Spectroscopy, JACS Au. 2 (2022) 787–792.

[92] F. Göltl, S. Bhandari, M. Mavrikakis, Thermodynamics Perspective on the Stepwise Conversion of Methane to Methanol over Cu-Exchanged SSZ-13, ACS Catal. 11 (2021) 7719–7734. https://doi.org/10.1021/acscatal.1c00691.

[93] P. Da Costa, B. Modén, G.D. Meitzner, D.K. Lee, E. Iglesia, Spectroscopic and chemical characterization of active and inactive Cu species in NO decomposition catalysts based on Cu-ZSM5, Phys. Chem. Chem. Phys. 4 (2002) 4590–4601. https://doi.org/10.1039/b203700a.

[94] B. Ipek, M.J. Wulfers, H. Kim, F. Göltl, I. Hermans, J.P. Smith, K.S. Booksh, C.M. Brown, R.F. Lobo, Formation of $[Cu_2O_2]^{2+}$ and $[Cu_2O]^{2+}$ toward C-H Bond Activation in Cu-SSZ-13 and Cu-SSZ-39, ACS Catal. 7 (2017) 4291–4303.

https://doi.org/10.1021/acscatal.6b03005.

[95] D.J. Deka, R. Daya, A. Ladshaw, D. Trandal, S.Y. Joshi, W.P. Partridge, Assessing impact of real-world aging on Cu-redox half cycles of a Cu-SSZ-13 SCR catalyst via transient response measurements and kinetic modeling, Appl. Catal. B Environ. 309 (2022) 121233. https://doi.org/10.1016/j.apcatb.2022.121233.

[96] P.S. Dhillon, M.P. Harold, D. Wang, A. Kumar, S.Y. Joshi, Enhanced transport in washcoated monoliths: Application to selective lean $NO_x$ reduction and ammonia oxidation, Chem. Eng. J. 377 (2019) 119734. https://doi.org/10.1016/j.cej.2018.08.120.

[97] H.S. Fogler, Elements of Chemical Reaction Engineering, Third, 2004.

[98] I. Malpartida, O. Marie, P. Bazin, M. Daturi, X. Jeandel, An operando IR study of the unburnt HC effect on the activity of a commercial automotive catalyst for $NH_3$-SCR, Appl. Catal. B Environ. 102 (2011) 190–200. https://doi.org/10.1016/j.apcatb.2010.11.041.

[99] A. Kumar, K. Kamasamudram, A. Yezerets, Hydrocarbon Storage on Small-Pore Cu-Zeolite SCR Catalyst, SAE Int. J. Engines. 6 (2013) 680–687. https://doi.org/10.4271/2013-01-0508.

[100] I. Heo, Y. Lee, I.S. Nam, J.W. Choung, J.H. Lee, H.J. Kim, Effect of hydrocarbon slip on NO removal activity of CuZSM5, FeZSM5 and $V_2O_5/TiO_2$ catalysts by $NH_3$, Microporous Mesoporous Mater. 141 (2011) 8–15. https://doi.org/10.1016/j.micromeso.2010.02.005.

[101] J.-Y. Luo, O. Harry, C. Henry, W. Epling, Effect of $C_3H_6$ on selective catalytic reduction of $NO_x$ by $NH_3$ over a Cu/zeolite catalyst: A mechanistic study, Appl. Catal. B Environ. (2012) 296–305. https://doi.org/10.1016/j.apcatb.2008.07.001.

[102] H. Zhao, X. Wu, Z. Huang, H. Shen, J. Dong, X. Li, G. Jing, Changes of the $C_3H_6$-Poisoning Effect over a Cu-SSZ-13 NH3-SCR Catalyst upon Hydrothermal Treatment at Different Temperatures, Energy and Fuels. 36 (2022) 2712–2721. https://doi.org/10.1021/acs.energyfuels.1c04336.

[103] C. He, Y. Wang, Y. Cheng, C.K. Lambert, R.T. Yang, Activity, stability and hydrocarbon deactivation of Fe/Beta catalyst for SCR of NO with ammonia, Appl. Catal. A Gen. 368 (2009) 121–126. https://doi.org/10.1016/j.apcata.2009.08.020.

[104] L. Ma, W. Su, Z. Li, J. Li, L. Fu, J. Hao, Mechanism of propene poisoning on Cu-SSZ-13 catalysts for SCR of $NO_x$ with $NH_3$, Catal. Today. 245 (2015) 16–21. https://doi.org/10.1016/j.cattod.2014.05.027.

**Appendix A. Supporting Information of Chapter 2. How Changes in Cu-SSZ-13 Catalytic Oxidation Activity via Mild Hydrothermal Aging Influence Sulfur Poisoning Extents**

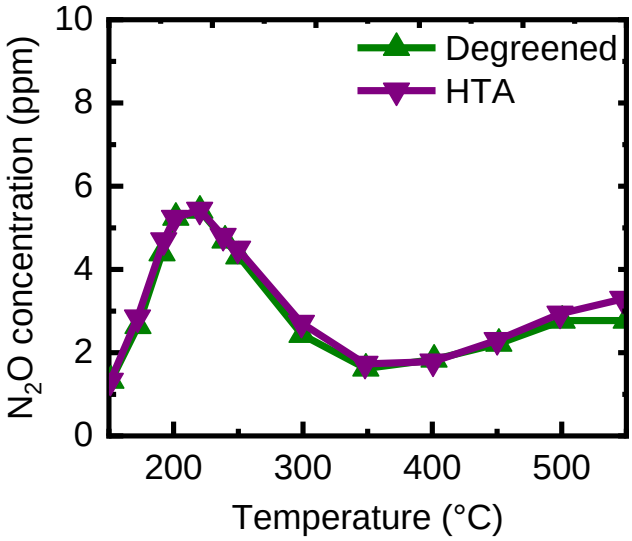


Fig. A.1. $N_2O$ formation comparison between degreened and HTA pretreated Cu-SSZ-13 catalysts during $NH_3$-SCR reactions.

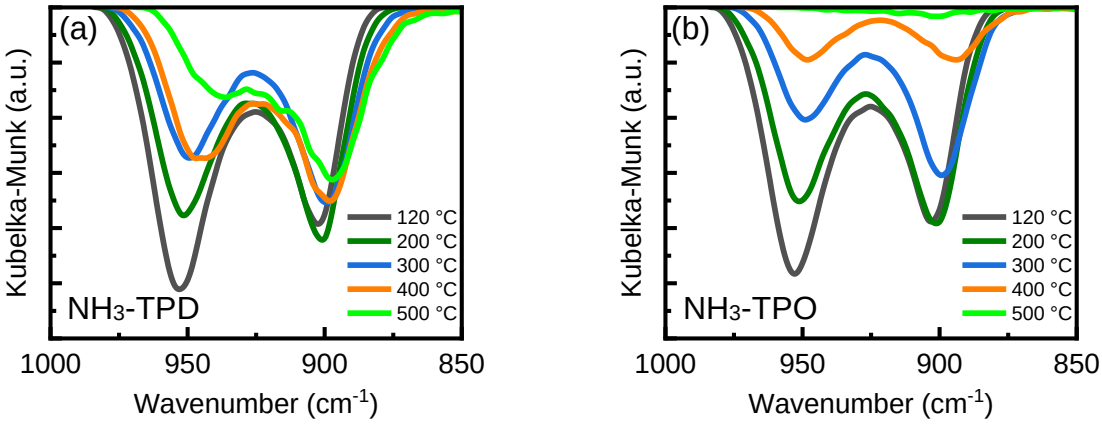


Fig. A.2. DRIFTS results obtained during (a) $NH_3$-TPD and (b) $NH_3$-TPO experiments on the Cu-SSZ-13 catalyst after scraping from a monolith brick. Both experiments were conducted after oxygen pretreated at 500 °C for 1 h, cooling to 120 °C in He and then 1000 ppm $NH_3$ balance in

He. For the TPD, He was used while 10% $O_2$ balance in He was used in the TPO experiment. The temperature ramp was 10 °C/min.

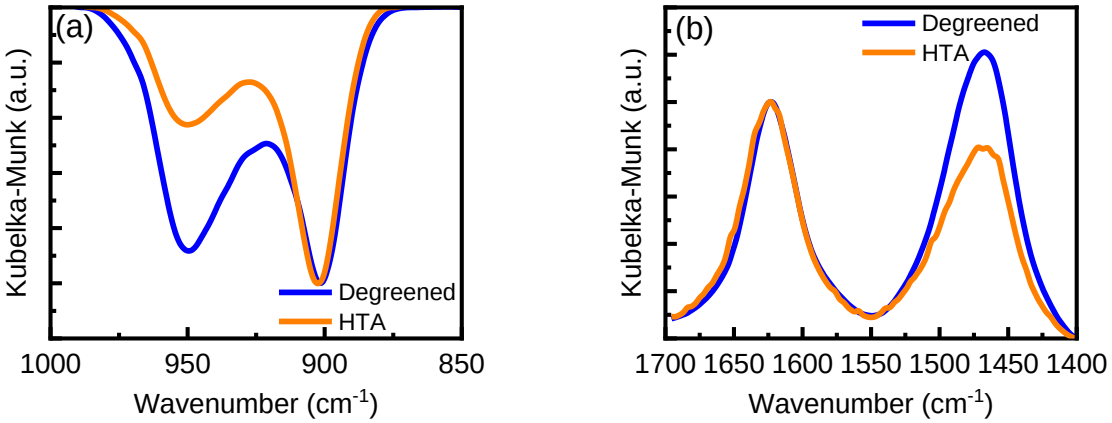


Fig. A.3. DRIFTS $NH_3$ adsorption spectra comparison between the degreened and HTA catalysts in (a) the T-O-T vibration region and (b) the Brønsted and Lewis acid sites region. The spectra were normalized separately in these two regions. In (a), the spectra were normalized using the 900 $cm^{-1}$ feature while in (b), the spectra were normalized using the 1620 $cm^{-1}$ feature.

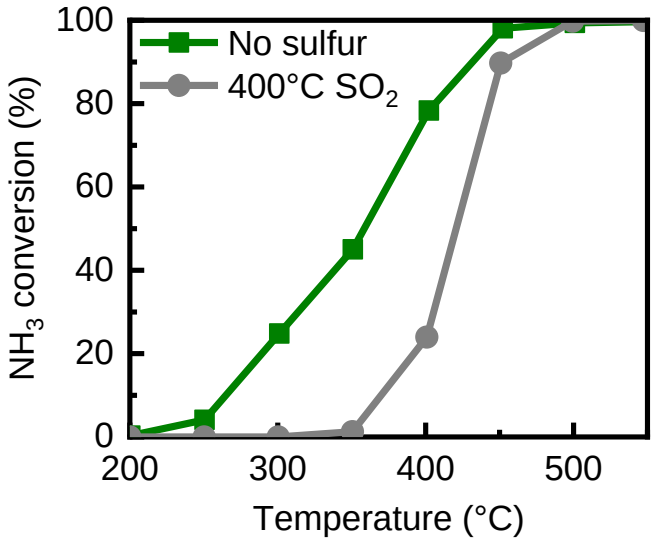


Fig. A.4. $NH_3$ oxidation conversion over the degreened catalyst before and after sulfur exposure at 400 °C $SO_2$. During the $NH_3$ oxidation experiment, 10% $O_2$, 7% $H_2O$, 8% $CO_2$, 200 ppm $NH_3$ and balance in $N_2$ were used.

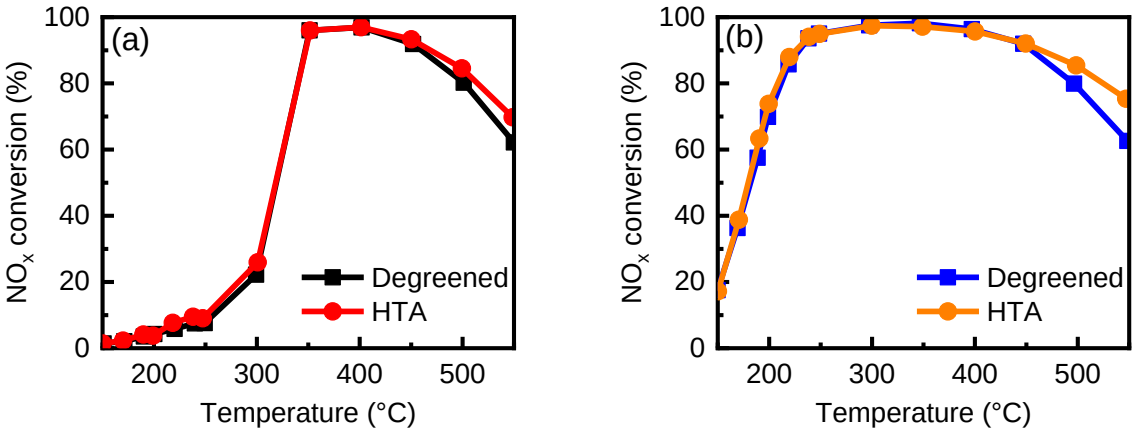


Fig. A.5. A comparison of SCR results after (a) 25 ppm $SO_2$ and 25 ppm $SO_3$ exposure at 200 °C and after (b) 50 ppm $SO_2$ exposure at 200 °C for the degreened and HTA catalysts. The SCR reaction conditions are described in Table 1.

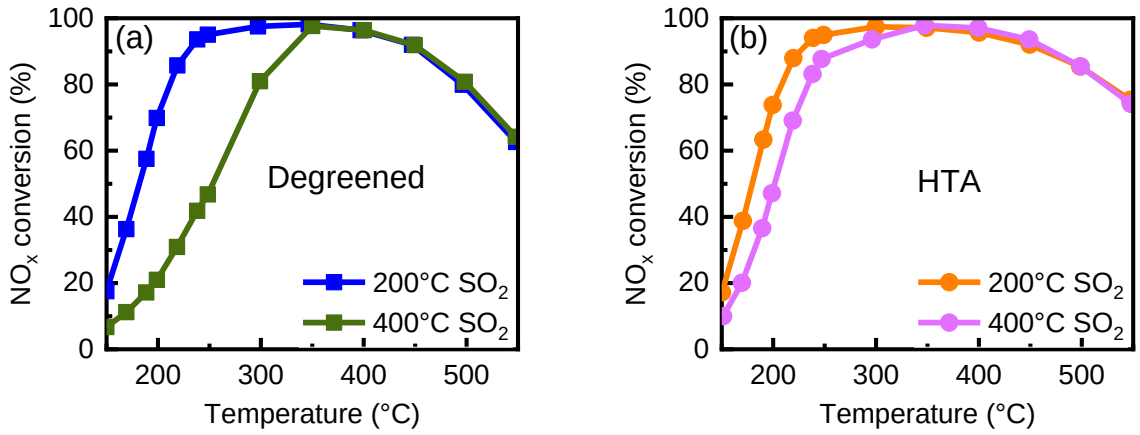


Fig. A.6. A comparison of SCR results after a 50 ppm $SO_2$ exposure at 200 and 400 °C on the (a) degreened and (b) HTA catalysts. The SCR reaction conditions are described in Table 1.

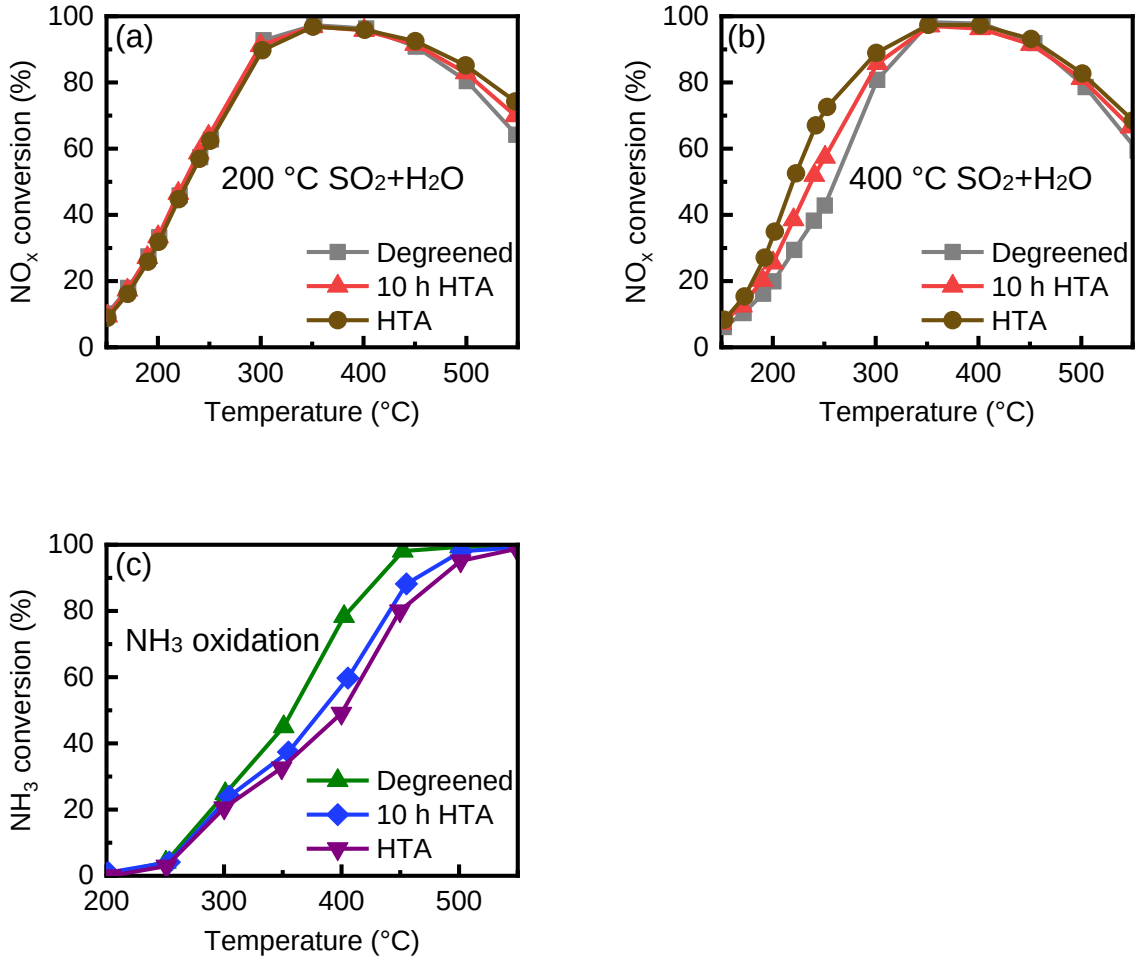


Fig. A.7. A comparison of degreened, 10 h HTA and HTA (for 25 h) after (a) 200 °C and (b) 400 °C $SO_2$ + $H_2O$ exposure. The $NH_3$ oxidation comparison before sulfur exposure between three samples is shown in (c). The SCR and $NH_3$ oxidation conditions are listed in the experimental methods session.

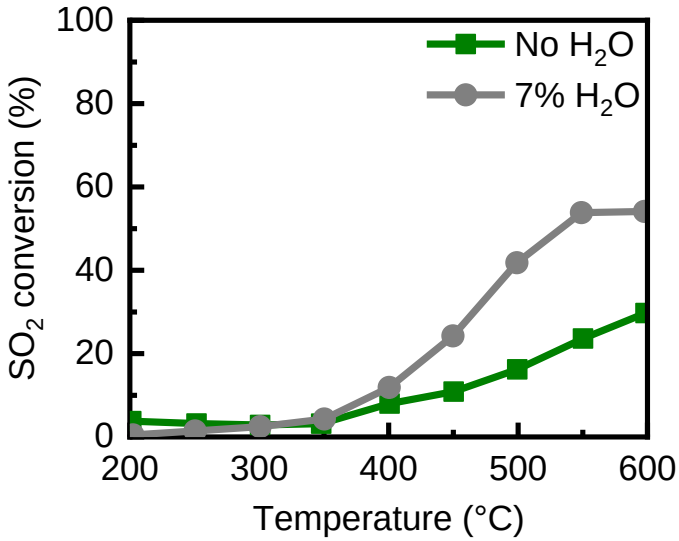


Fig. A.8. $SO_2$ oxidation over the degreened catalyst. The $SO_2$ oxidation conditions in the absence of water were 50 ppm $SO_2$, 10% $O_2$ and balance in $N_2$ and the $SO_2$ oxidation conditions in the presence of water were 50 ppm $SO_2$, 10% $O_2$, 7% $H_2O$ and balance in $N_2$.